QUANTUM NOISE AND MEASURING QUANTUM DISTANCE FOR NISQ CIRCUITS

Md Sakibul Islam
Graduate Research Fellow
Bangladesh Reference Institute for Chemical Measurements
75 Laboratory Rd, Dhaka 1205, Bangladesh
sakibulislamsazzad@gmail.com

Protik Nag
Department of Computer Science Engineering
Shahjalal University of Science and Technology
Sylhet, Bangladesh-3114
protik22@student.sust.edu

ABSTRACT

Present day quantum computers suffer from a plethora of errors such as gate error, readout error, relaxation and dephasing error, and crosstalk. Therefore, they are often known as noisy intermediate-scale quantum (NISQ) computers. In this article, we analyzed the performance of several classes of quantum circuits under various errors. We executed NISQ circuits on both noisy simulator and real hardware backend publicly available from IBM Quantum. On simulation, we created noise models with both individual errors and combination of multiple errors to quantify how each type of error impact performance of quantum circuits. We utilized statistical distances such as total variation distance (TVD), Jensen-Shannon divergence (JSD), and Hellinger distance, to measure the deviation of noisy output from ideal output. Finally, we compare the noisy outputs from the simulator and outputs from the real hardware to showcase the gap between simulation and real device experiment. This gap points to the limitation of present noise models failure to exhibit the behavior of real hardware.

1 Introduction

Quantum computing has become popular in recent years. Both investment and research on quantum computing have been increased in past few years. As the interest grows, more hardwares are being developed [1]. With the increasing number of quantum hardwares, the necessity to analyze their performance is also rising. Existing NISQ circuits are errors prone and mainly they are noisy. Errors happening due to noise make subtle performance challenging for quantum computing and also hindering the scalability of this technology. One of the most prominent source of error is noisy interactions between quantum hardware and its surrounding environment. Interaction between quantum circuits and environments are commonly known as decoherence. There are also several sources that can cause noise like controlling pulses, heat, even impurities exists in the qubit materials. As a result, a separate domain of interest emerged to mitigate the impact of noise.

Quantum noise exhibits a statistical distribution [2]. Hence researchers have put their efforts to understand the impact of noise by analysing its statistical properties. Even analyzing noise effects sometimes enhance qubit information processes due to its stochastic behavior [3]. Stochastic analysis is convenient to understand the source of *Gaussian Noise* [4]. Basically Gaussian noise occurs due to a large number of random noise sources. Hence, it is quite difficult to figure out the noise sources and to pull it out as a distinct source of noise. Separating noise from gaussian background noise can extract the only relevant high-order noise using signal processing help to understand more specific types of noise. This resultant noise signals are described as *Non-Gaussian noise*. This reconstructions can help to build more robust noise model that mimics realistic qubit errors, cause in reality non-gaussian noise [5]. Another good approach to mimic noise exists in a quantum system is to analyse the noise and try to find out a pattern of it [6].

Impact of quantum noise adversely affect performance. Performance of a quantum system due to noise can be analysed by quantum benchmarking. In this study [7], the authors have provided numerical simulations regarding quantum benchmarking and discussed several challenges. According to them, benchmarking task can sometimes be misleading. It becomes more complicated when we try to benchmark a quantum machine or a quantum program. Quantum computers are more diverse but yet less developed. Again, quantum noises are difficult to replicate which makes it challenging to benchmark them. Authors in this study suggested trace distance (a generalization for total variational distance [8]) and

Hellinger distance as metrics to benchmark quantum machines. In our study, we included Jensen-Shannon Divergence to measure the distance between actual quantum output and ideal quantum output.

Hardware-agnostic benchmarking suite also exists [9]. The authors considered different aspects of a noisy quantum machine like parallelism, entanglement-ratio, critical-depth, adaptability based on the use-case application of quantum program. In this study, we mimicked their hardware design features against our noise model on seven of the NISQ circuits they used, namely GHZ state, Mermin-Bell state, Phase Code, Bit Code, QAOA (both Swap QAOA and Vanilla QAOA) and Hamiltonian Simulation. There are several works on randomized quantum benchmarking [10, 11]. They alleviate the problem with quantum process tomography which scales exponentially with the number of qubits. These methods can calculate the average error rate from QPUs native gates. Among synthetic benchmarking models there are quantum volume protocol and LINPACK benchmarking [12]. However, both of them have scalability issues [9]. Finally, there is application level benchmarking. The Variational Quantum Eigensolver (VQE) and Quantum Approximate Optimization Algorithm (QAOA) are considered as application level quantum benchmark.

Current quantum computing hardware widely ranged as photonics, superconducting and trapped ion architectures [13]. On this work, we considered a set of programs (quantum circuits) for generic noise models that exist on almost all quantum computer architectures. Later, we analyzed the noisy simulation with ideal simulation and real device experiment in terms of statistical distances. Moreover, we have been able to calculate diamond norm till 3 qubits for a noise model of depolarising error and reset error. For single qubit, two qubits and three qubits depolarising error diamond norm value is respectively 0.99999638, 1.00000170, 1.000053479 (eight significant value is considered). In case of reset error value, diamond norm value is 0.999998561 for all three qubit cases. Same initial condition for all qubits is the reason behind of identical reset error value.

2 Background

Typically, for studying a noise model a set of quantum circuits are chosen based on the preferences. Here, most common few NISQ circuits are selected. Each circuit addresses particular quantum aspects e.g., entanglement, bell inequality etc. Our main contribution in the article is to make a noise model that addresses three different errors i.e., Bit Flip error, Depolarising error, Thermal Error. Noisy simulations on the selected NISQ circuits provide results in a probability distributions output. To check the perfectness of the noise model, probability distribution distance between ideal and noisy simulated model are calculated. Measuring probability distribution distance, i.e., *Quantum Distance* demonstrates the fidelity of ideal circuit and make a comparison between ideal and noisy simulators. Mostly, they are known as *Distance Metrics*. For this article, three *Distance Metrics* are formulated for finding the disperse between noisy simulation and ideal simulator output and comparison are made in between them. We also made an experimental simulation on IBM Quantum real device *open* backends.

Output states of the circuits are created on an ideal Simulator provided by IBM Qiskit backend, `AerSimulator`. *Bit flip, Thermal and Depolarising error* are considered for comparing the ideal and noisy simulator output states. Probability distribution of the output states are then considered for quantum distance.

2.1 NISQ Circuits

2.1.1 GHZ

Measuring GHZ states exhibits entanglement generation of a quantum processor. GHZ circuit consists of Hadamard gate following a sequence of CNOT gate which produce entangled state [14]:

$$[H]|\psi\rangle = \frac{|000\rangle + |111\rangle}{\sqrt{2}} \tag{1}$$

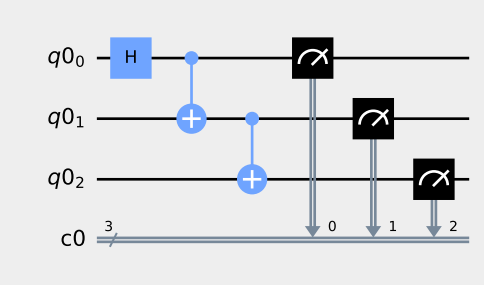

Figure 1: Circuit for GHZ State

2.1.2 Mermin Bell

Mermin bell circuit is a generalization of GHZ state to test Bell inequality by measuring Mermin Polynomial operator [15]. Mermin inequality is a test of checking fidelity of a quantum processor. Mermin Polynomial operator expectation value is measured by:

$$M = \frac{1}{2i}(\prod_{j=1}^{n}(\sigma_x^j + i\sigma_y^j) - (\sigma_x^j - i\sigma_y^j)) \tag{2}$$

Here, σ_x^j and σ_y^j are Pauli-X and Pauli-Y operators are acting on j-th qubit. Expectation value of this operator should be $\langle\psi|M|\psi\rangle = 2^{n-1}$ For n-qubit system.

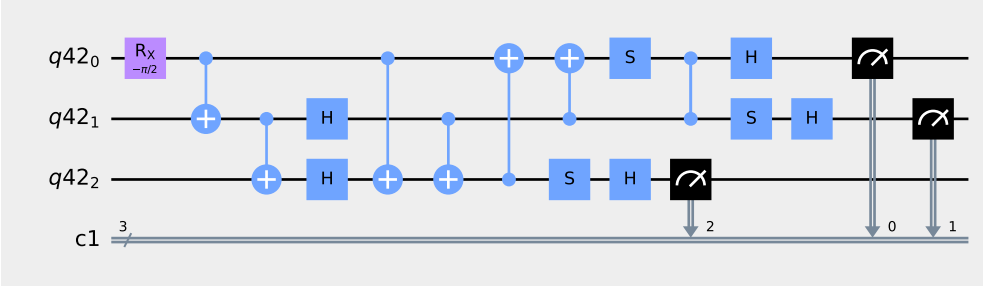

Figure 2: Mermin Bell Circuit

2.1.3 Phase Code

Phase code is parameterized by data qubits with phase flip repetition code. In this work, a sample circuit is created with initial state of $|+\rangle = \frac{|0\rangle+|1\rangle}{\sqrt{2}}$ and $|-\rangle = \frac{|0\rangle-|1\rangle}{\sqrt{2}}$ with r significant values of error correction and final state is measured. In a noiseless setting the final states should be identical to the initial states [16].

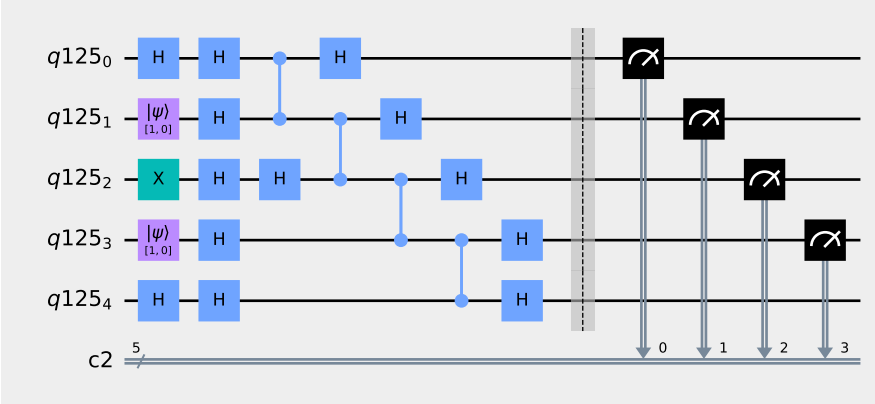

Figure 3: Circuit for Phase Code

2.1.4 Bit Code

Bit code is as same as Phase code that is parameterized by data qubits. Instead of phase flip, Bit code flip bits with a r round error correction.

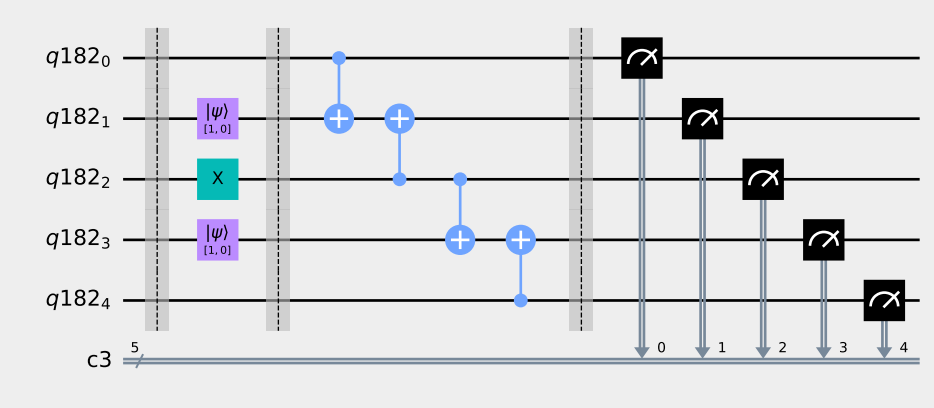

Figure 4: Circuit for Bit Code

2.1.5 QAOA

Quantum Approximate Optimization Algorithm (QAOA) is trained to solve combinatorial optimization problems. In this work QAOA is designed for Max-cut problem with an edge weight {-1,+1}. This type of Max-cut is commonly known as Sherrington-Kirkpatrick (SK) model. SK model is perfectly depicted in the Vanilla QAOA ansatz circuit. Hence, the Vanilla QAOA circuit follows all-to-all connectivity. There is a natural choice of solving Max-cut and ansatz of ZZ-SWAP QAOA is created by interaction between every pair of qubits, $n(n-1)/2$ edges [17] [18].

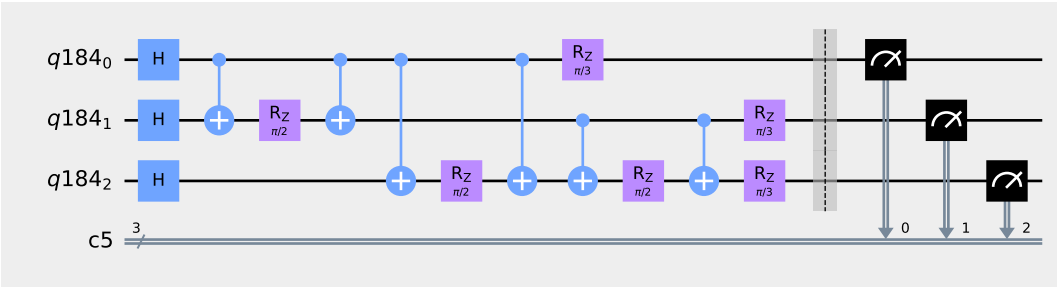

Figure 5: Vanilla QAOA Circuit Implementation

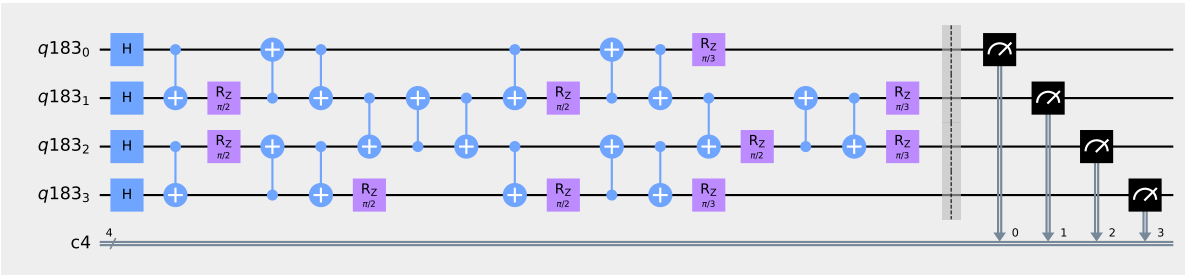

Figure 6: Swap QAOA Circuit Implementation

2.1.6 Hamiltonian Simulation

For Hamiltonian simulation, we considered the following Hamiltonian of 1D TFIM system consist of N spin qubits

$$H = -\sum_{i=1}^{N} \left[J_z \sigma_z^i \sigma_z^{i+1} + \epsilon_{ph} cos(\omega_{ph} t) \sigma_x^i \right] \tag{3}$$

Here, J_z is a coupling constant signifies nearest-neighbor interaction strength and $\epsilon_{ph} cos(\omega_{ph} t))$ describes time varying magnetic field [19] [20].

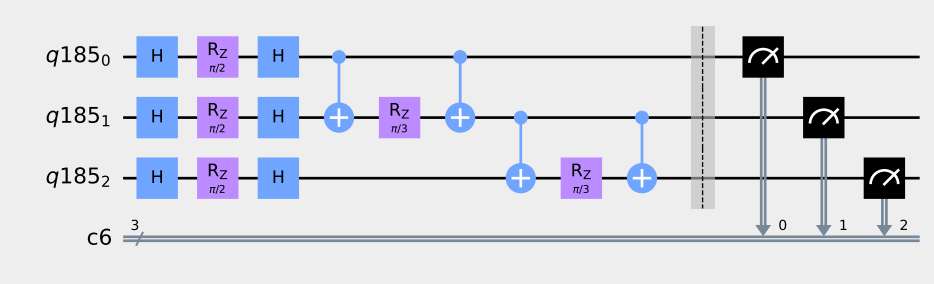

Figure 7: Hamiltonian Circuit Implementation

2.2 Noise Model

To simulate quantum circuits with noise, we utilize three noise models, namely, bit-flip error, thermal noise (T1-relaxation and T2-dephasing), and depolarizing noise. Readout errors are also considered for thermal and depolarizing noise simulations.

2.2.1 Bit Flip Error

For a bit flip error noise model are considered in following cases:

- For a single qubit gate, probability of flipping the state.
- For two qubit gates, applying single qubit bit-flip errors for each one.
- During resetting, probability of resetting to 1 instead of 0.
- In case of measuring, probability of flipping the state is considered.

2.2.2 Thermal Noise Model

For a thermal noise channel, each qubit is parameterized by a thermal relaxation time constant T1 and dephasing time constant T2. For a valid parameterization, $T2 \leq 2T_1$ must be true. Violation of this inequality, makes the error channel as unitary and mixed reset for $T_2 \leq T_1$. In case of $T_1 < T_2 \leq 2T_1$ can be expressed as Kraus error channel [21].

2.2.3 Depolarizing

Depolarizing error channel can be defined as [22]

$$E(\rho) = (1 - \lambda)\rho + \lambda Tr(\rho) \frac{I}{2^n} \tag{4}$$

Here, λ is error parameter and n is the number of qubits [23], where value of λ ranges from $0 \leq \lambda \leq \frac{4^n}{4^n - 1}$

- If λ=0, then it is an identity channel $E(\rho) = \rho$
- If $\lambda = 1$, it is completely depolarizing channel $E(\rho) = \frac{I}{7} 2^n$
- If $\lambda = \frac{4^n}{(4^n - 1)}$, it can be defined as uniform Pauli Error Channel, $E(\rho) = \sum_j (P_j \rho P_j)/(4^n - 1)$ for all $P_j ! = I$ For this work, $\lambda = 0.1$ is considered.

2.3 Distance Metrics

In this work, we use statistical distance metrics to compare two sets of output distributions. Primarily, distances are measured by *Total Variational Distance* (TVD). For a *n* qubit output states has $N = 2^n$ states and TVD can be calculated by the following formulation:

$$\frac{1}{2}\sum_{k=1}^{k=N}|p(k) - p'(k)| \tag{5}$$

Here, $p(k)$ is the probability of the states k with the ideal circuits and $p'(k)$ is the probability of states k with the noisy circuits [24].

Another distance metric considered for this work is *Jensen-Shannon Divergence*. which is formulated by the following equation:

$$\sqrt{\frac{1}{2}[D(p||m) + D(p'||m)]} \tag{6}$$

Here, *m* is the point-wise mean of p and p'. D is the Kullback-Leibler divergence defined as [25]

$$\sum_k q(k)log(\frac{q(k)}{r(k)}) \tag{7}$$

where, q and r is the two probability distribution. All of the mentioned distance are ranged between 0 and 1, where 0 is the best case meaning no difference between ideal and noisy case.

We use another metric named *Hellinger Distance*. Hellinger distance is the equivalence of Euclidean Distance. For two probability distribution of P and Q. Formally, Hellinger distance is defined as:

$$h(P, Q) = \frac{1}{\sqrt{2}}\|\sqrt{P} - \sqrt{Q}\| \tag{8}$$

In our study *hellinger distance* modules provided by Qiskit package is formulated to compare the difference between ideal and noisy simulations [26]. It is the performance metric to make comparison of ideal and experimentally distributed probability distribution.

3 Results and Discussion

Main goal of the project was to check the error-prone characteristics of the NISQ circuits and demonstrate them in a table (Table 1 and Table 2). Noise models are simulated for each errors. Parameters for the models are chosen by following state of the art. To make a bare eye comparison, output states histograms are plotted against ideal simulator provided by *Qiskit*, *AerSimulator*. Simulated histogram plots are available in SI.

3.0.1 Discussion

For each kind of error, we can see that the mismatches between ideal and simulated states for GHZ state, Mermin Bell state, Phase Code state and Bit code state can be identified with bare eyes. But Swap QAOA, Vanilla QAOA and Hamiltonian states produces so much noises. To measure and compare the outputs, we have to relay on the distance metrics explained earlier 2.3. The table 1 below compares the distance values for each states when introduced to different types of errors.

State Name	Error	TVD	JSD	Hellinger
GHZ	Bit Error	0.552734	0.671626	0.575589
	Thermal Error	0.055664	0.826572	0.168860
	Depolarizing Error	0.137695	0.768309	0.267204
Mermin	Bit Error	0.745117	0.745375	0.703662
	Thermal Error	0.078125	0.828298	0.199642
	Depolarizing Error	0.151367	0.821676	0.280691
Phase	Bit Error	0.433594	0.718665	0.498318
	Thermal Error	0.059570	0.800651	0.165148
	Depolarizing Error	0.094727	0.783709	0.220902
Bit	Bit Error	0.778320	0.826520	0.727442
	Thermal Error	0.083008	0.781994	0.205920
	Depolarizing Error	0.236328	0.830225	0.355129
Swap QAOA	Bit Error	0.068359	0.048867	0.059550
	Thermal Error	0.081055	0.062997	0.069029
	Depolarizing Error	0.048828	0.052720	0.045072
Vanilla QAOA	Bit Error	0.040039	0.039797	0.032238
	Thermal Error	0.044922	0.074000	0.038908
	Depolarizing Error	0.058594	0.065567	0.047182
Hamiltonian	Bit Error	0.043945	0.047421	0.041027
	Thermal Error	0.058594	0.076158	0.048010
	Depolarizing Error	0.043945	0.051197	0.043118

Table 1: States-Error vs Distances Table

Table 2 represents the distance data for states ran on real devices.

Real Device	State Name	TVD	JSD	Hellinger
ibmq_belem	bit_circ	0.317195	0.798787	0.336362
	ghz_circ	0.093773	0.751159	0.154430
	hamilton_circ	0.091883	0.073828	0.074095
	mermin_circ	0.791398	0.493197	0.659724
	phase_circ	0.184922	0.500122	0.218252
	swap_qaoa_circ	0.088781	0.095780	0.084936
	vanilla_qaoa_circ	0.131883	0.121733	0.104710
ibmq_lima	bit_circ	0.115797	0.792652	0.209068
	ghz_circ	0.044758	0.772231	0.101447
	hamilton_circ	0.102664	0.086657	0.076724
	mermin_circ	0.139664	0.704546	0.160856
	phase_circ	0.110734	0.673815	0.155431
	swap_qaoa_circ	0.071945	0.085265	0.064208
	vanilla_qaoa_circ	0.096383	0.073539	0.077338
ibmq_manila	bit_circ	0.077742	0.804447	0.157350
	ghz_circ	0.073094	0.773956	0.137056
	hamilton_circ	0.028898	0.043327	0.030037
	mermin_circ	0.156469	0.741374	0.189601
	phase_circ	0.067961	0.523871	0.125884
	swap_qaoa_circ	0.068727	0.088215	0.058530
	vanilla_qaoa_circ	0.088219	0.073094	0.071136
	bit_circ	0.129219	0.807277	0.205142

Table 2 continued from previous page

Real Device	State Name	TVD	JSD	Hellinger
ibmq_nairobi	ghz_circ	0.081984	0.749682	0.126361
	hamilton_circ	0.105219	0.083323	0.086210
	mermin_circ	0.254172	0.720565	0.234390
	phase_circ	0.082781	0.477326	0.141343
	swap_qaoa_circ	0.097039	0.087765	0.080030
	vanilla_qaoa_circ	0.121594	0.096839	0.097454
ibmq_oslo	bit_circ	0.158500	0.785755	0.223138
	ghz_circ	0.072742	0.742672	0.185708
	hamilton_circ	0.086461	0.047587	0.077877
	mermin_circ	0.216305	0.749358	0.269299
	phase_circ	0.091758	0.723172	0.142515
	swap_qaoa_circ	0.127008	0.086468	0.109444
	vanilla_qaoa_circ	0.082047	0.054443	0.068577
ibmq_quito	bit_circ	0.142758	0.793755	0.228152
	ghz_circ	0.156867	0.696616	0.220118
	hamilton_circ	0.096469	0.075148	0.072665
	mermin_circ	0.316469	0.659058	0.304724
	phase_circ	0.179688	0.622409	0.218213
	swap_qaoa_circ	0.074375	0.108501	0.066640
	vanilla_qaoa_circ	0.127969	0.117088	0.125604

Table 2: Device Name-State vs Distance Table

4 Conclusion

By comparing Table 1 and Table 2, we can make say that current noise models cant mimic a real quantum processor. Main challenges for current state of the art is to consider all noise dynamics for a hardware quantum processor.

Codes are available on this repository: Github Repository

References

[1] Salonik Resch and Ulya R Karpuzcu. Quantum computing: an overview across the system stack. *arXiv preprint arXiv:1905.07240*, 2019.

[2] Crispin Gardiner, Peter Zoller, and Peter Zoller. *Quantum noise: a handbook of Markovian and non-Markovian quantum stochastic methods with applications to quantum optics*. Springer Science & Business Media, 2004.

[3] Nicolas Gillard, Etienne Belin, and François Chapeau-Blondeau. Enhancing qubit information with quantum thermal noise. *Physica A: Statistical Mechanics and its Applications*, 507:219–230, 2018.

[4] Crispin W Gardiner and Matthew J Collett. Input and output in damped quantum systems: Quantum stochastic differential equations and the master equation. *Physical Review A*, 31(6):3761, 1985.

[5] Youngkyu Sung, Félix Beaudoin, Leigh M Norris, Fei Yan, David K Kim, Jack Y Qiu, Uwe von Lüpke, Jonilyn L Yoder, Terry P Orlando, Simon Gustavsson, et al. Non-gaussian noise spectroscopy with a superconducting qubit sensor. *Nature communications*, 10(1):1–8, 2019.

[6] Scott E Smart, Zixuan Hu, Sabre Kais, and David A Mazziotti. Relaxation of stationary states on a quantum computer yields a unique spectroscopic fingerprint of the computer's noise. *Communications Physics*, 5(1):1–7, 2022.

[7] Salonik Resch and Ulya R Karpuzcu. Benchmarking quantum computers and the impact of quantum noise. *ACM Computing Surveys (CSUR)*, 54(7):1–35, 2021.

[8] F Ciccarello, T Tufarelli, and V Giovannetti. Toward computability of trace distance discord. *New Journal of Physics*, 16(1):013038, 2014.

[9] Teague Tomesh, Pranav Gokhale, Victory Omole, Gokul Subramanian Ravi, Kaitlin N Smith, Joshua Viszlai, Xin-Chuan Wu, Nikos Hardavellas, Margaret R Martonosi, and Frederic T Chong. Supermarq: A scalable quantum benchmark suite. In *2022 IEEE International Symposium on High-Performance Computer Architecture (HPCA)*, pages 587–603. IEEE, 2022.

[10] Easwar Magesan, Jay M Gambetta, and Joseph Emerson. Scalable and robust randomized benchmarking of quantum processes. *Physical review letters*, 106(18):180504, 2011.

[11] Timothy J Proctor, Arnaud Carignan-Dugas, Kenneth Rudinger, Erik Nielsen, Robin Blume-Kohout, and Kevin Young. Direct randomized benchmarking for multiqubit devices. *Physical review letters*, 123(3):030503, 2019.

[12] Yulong Dong and Lin Lin. Random circuit block-encoded matrix and a proposal of quantum linpack benchmark. *Physical Review A*, 103(6):062412, 2021.

[13] Arjan Cornelissen, Johannes Bausch, and András Gilyén. Scalable benchmarks for gate-based quantum computers. *arXiv preprint arXiv:2104.10698*, 2021.

[14] Yan Xia, Chang-Bao Fu, Shou Zhang, Suc-Kyoung Hong, Kyu-Hwang Yeon, and Chung-In Um. Quantum dialogue by using the ghz state. *arXiv preprint quant-ph/0601127*, 2006.

[15] Diego González, Diego Fernández de la Pradilla, and Guillermo González. Revisiting the experimental test of mermin's inequalities at ibmq. *International Journal of Theoretical Physics*, 59(12):3756–3768, 2020.

[16] Zijun Chen, Kevin J Satzinger, Juan Atalaya, Alexander N Korotkov, Andrew Dunsworth, Daniel Sank, Chris Quintana, Matt McEwen, Rami Barends, Paul V Klimov, et al. Exponential suppression of bit or phase flip errors with repetitive error correction. *arXiv preprint arXiv:2102.06132*, 2021.

[17] Michael Streif and Martin Leib. Training the quantum approximate optimization algorithm without access to a quantum processing unit. *Quantum Science and Technology*, 5(3):034008, 2020.

[18] Rishi Sreedhar. Qioa: Quantum inspired optimisation algorithm. 2021.

[19] Laura Clinton, Johannes Bausch, and Toby Cubitt. Hamiltonian simulation algorithms for near-term quantum hardware. *Nature communications*, 12(1):1–10, 2021.

[20] Zixuan Hu, Rongxin Xia, and Sabre Kais. A quantum algorithm for evolving open quantum dynamics on quantum computing devices. *Scientific reports*, 10(1):1–9, 2020.

[21] Man-Hong Yung. Thermal noise on adiabatic quantum computation. *arXiv preprint arXiv:0807.4819*, 2008.

[22] Miroslav Urbanek, Benjamin Nachman, Vincent R Pascuzzi, Andre He, Christian W Bauer, and Wibe A de Jong. Mitigating depolarizing noise on quantum computers with noise-estimation circuits. *Physical Review Letters*, 127(27):270502, 2021.

[23] Salman Beigi. Improved quantum hypercontractivity inequality for the qubit depolarizing channel. *Journal of Mathematical Physics*, 62(12):122201, 2021.

[24] Suresh Aakarshitha, Saki Abdullah Ash, Alam Mahababul, Onur Topaloglu Rasit, and Ghosh Swaroop. Short paper: A quantum circuit obfuscation methodology for security and privacy. In *Workshop on Hardware and Architectural Support for Security and Privacy*, pages 1–5, 2021.

[25] Hongtian Chen, Bin Jiang, and Ningyun Lu. An improved incipient fault detection method based on kullback-leibler divergence. *ISA transactions*, 79:127–136, 2018.

[26] Andrew Cross. The ibm q experience and qiskit open-source quantum computing software. In *APS March meeting abstracts*, volume 2018, pages L58–003, 2018.

5 Supplementary Information

Histogram plots are shown in here. Error bar plot is demonstrated for IBM devices. Quartile deviation is considered for error bar plot. Diamondd norm calculation is available in github repo. To calculate diamond norm a semi-definite process mentioned in the *Qiskit* SDK is used.

5.1 Bit Error

Bit errors are modelled for each qubit of the NISQ circuits. Gate error is also considered. In the histograms of this sections two legends are mentioned: *Ideal Probability*- simulation on Qiskit provided *AerSimulator* and *Calculated probability*- Output for bit error noise model simulation.

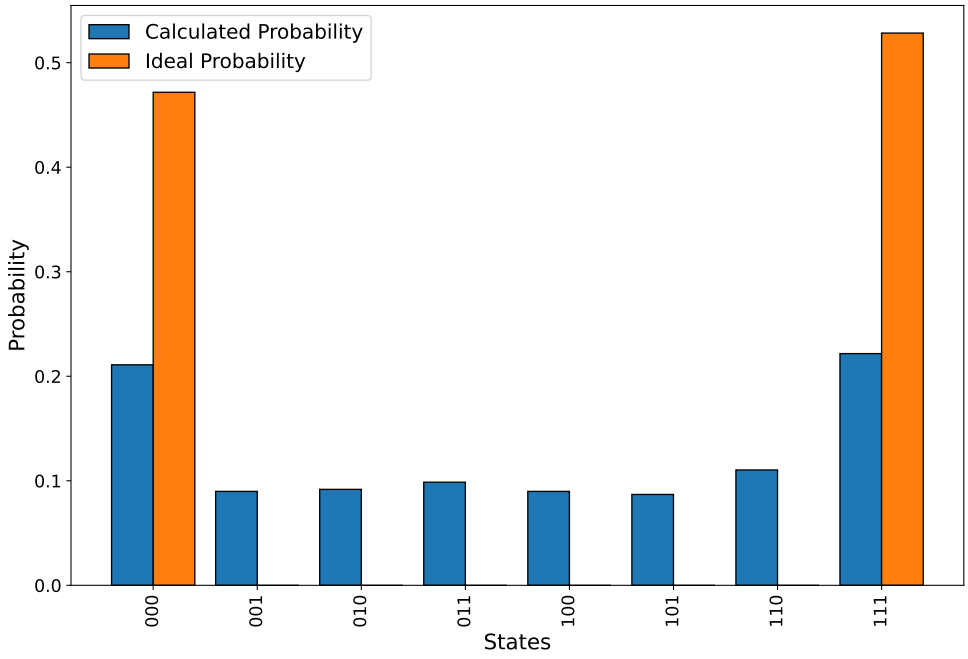

Figure 8: Impact of bit error on GHZ state

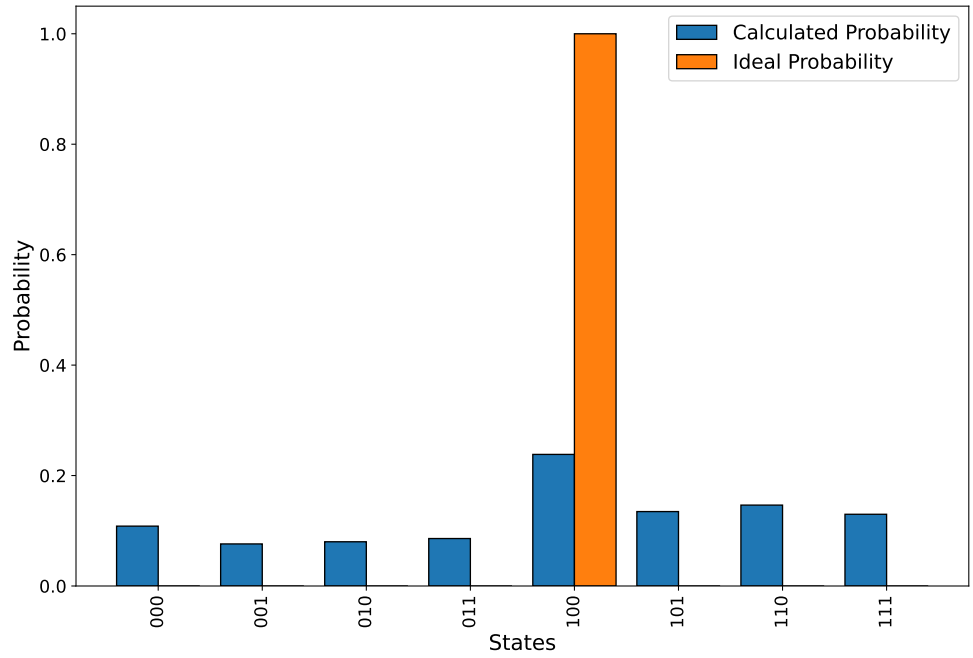

Figure 9: Impact of bit error on Mermin state

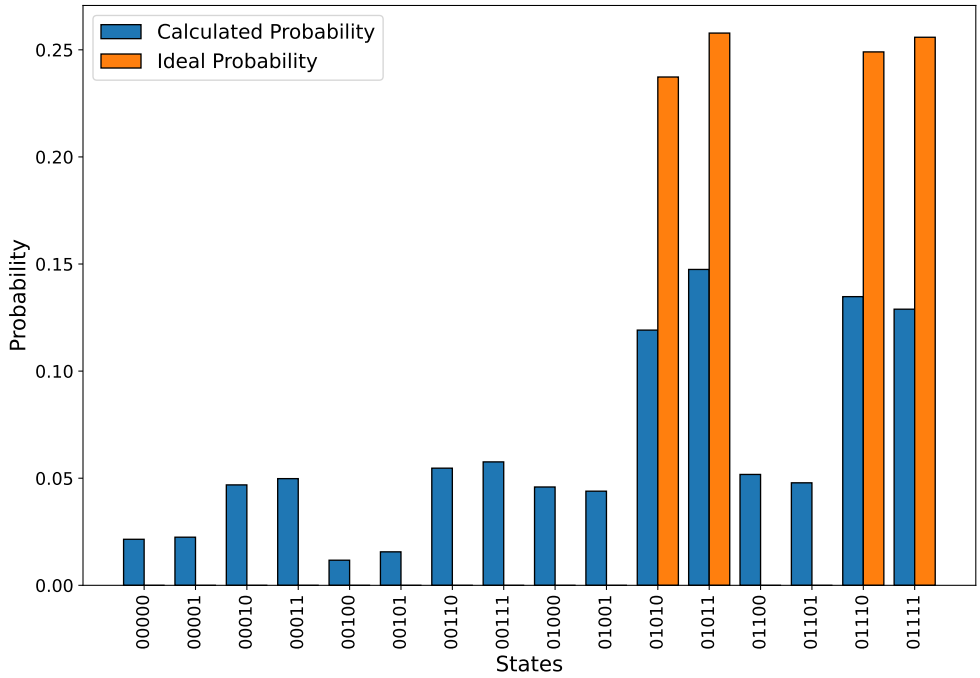

Figure 10: Impact of bit error on Phase Code state

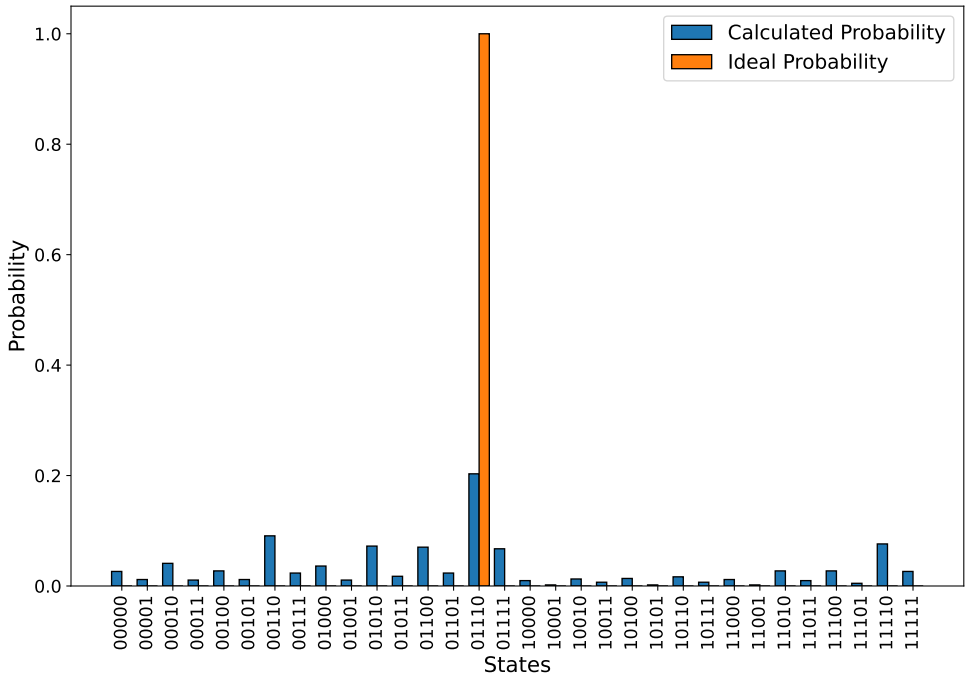

Figure 11: Impact of bit error on Bit Code state

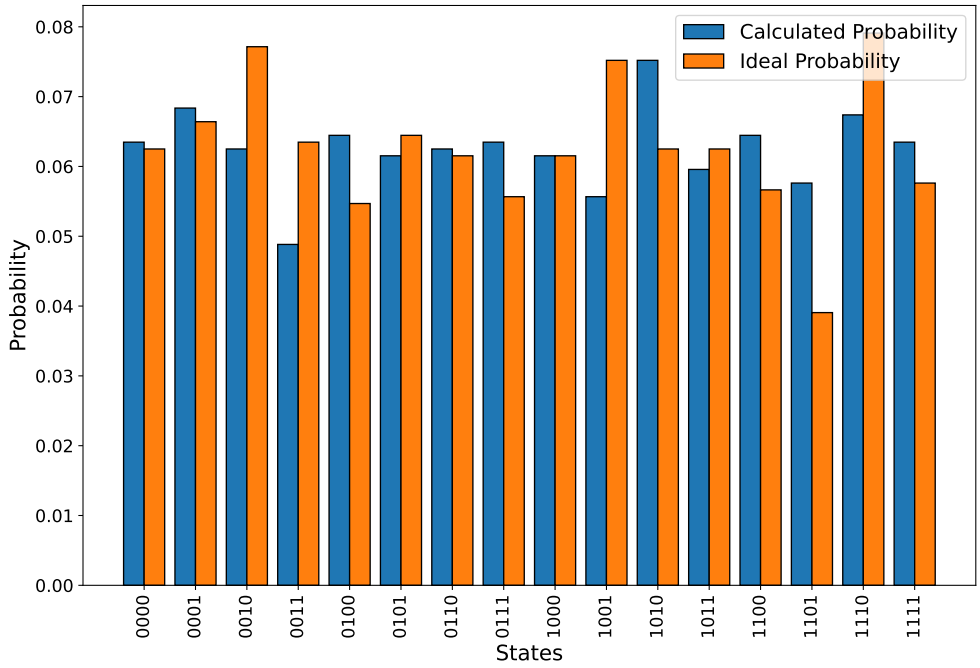

Figure 12: Impact of bit error on Swap QAOA state

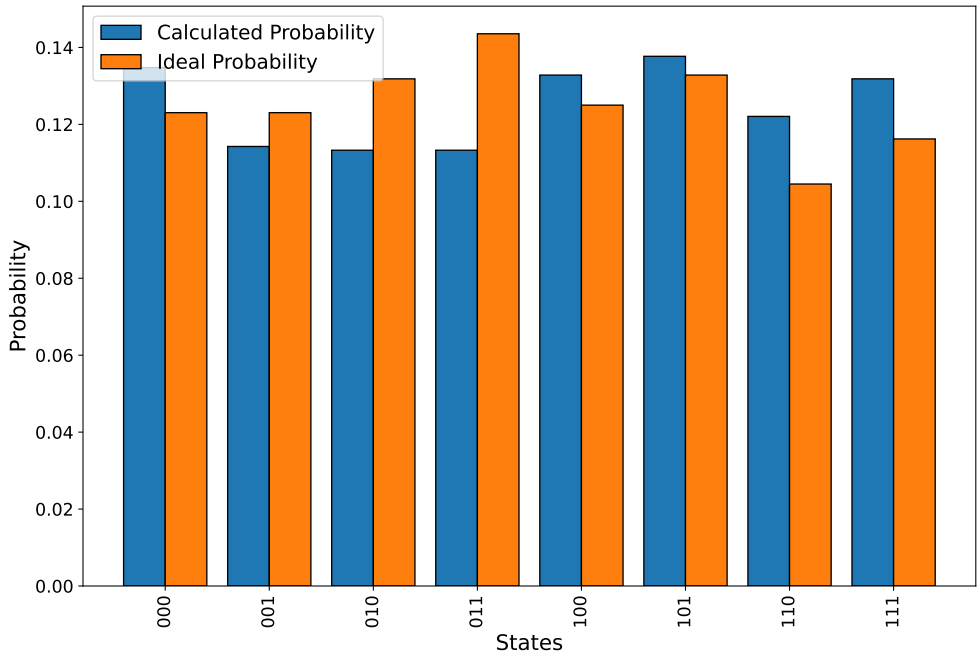

Figure 13: Impact of bit error on Vanilla QAOA state

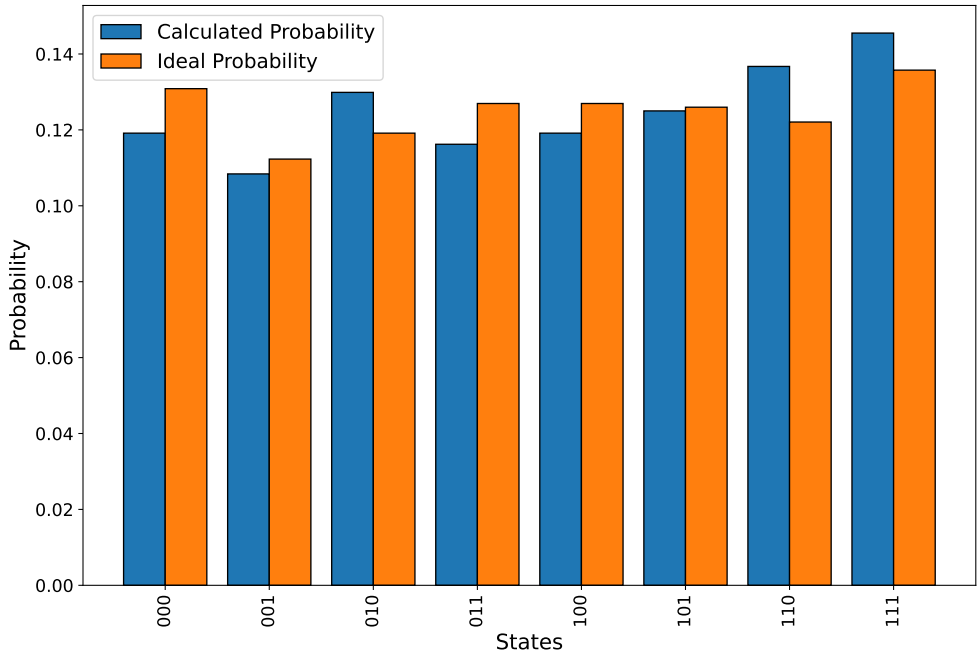

Figure 14: Impact of bit error on Hamiltonian state

5.2 Depolarizing Error

Qiskit provided module is used for depolarising error. Uniform Pauli Error Channel is chosen for the noise simulation.

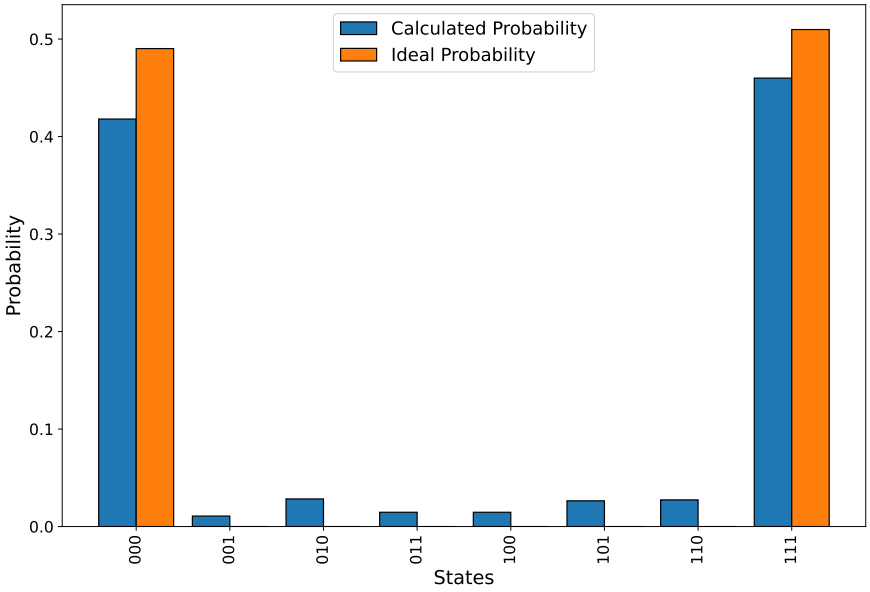

Figure 15: Impact of depolarizing error on GHZ state

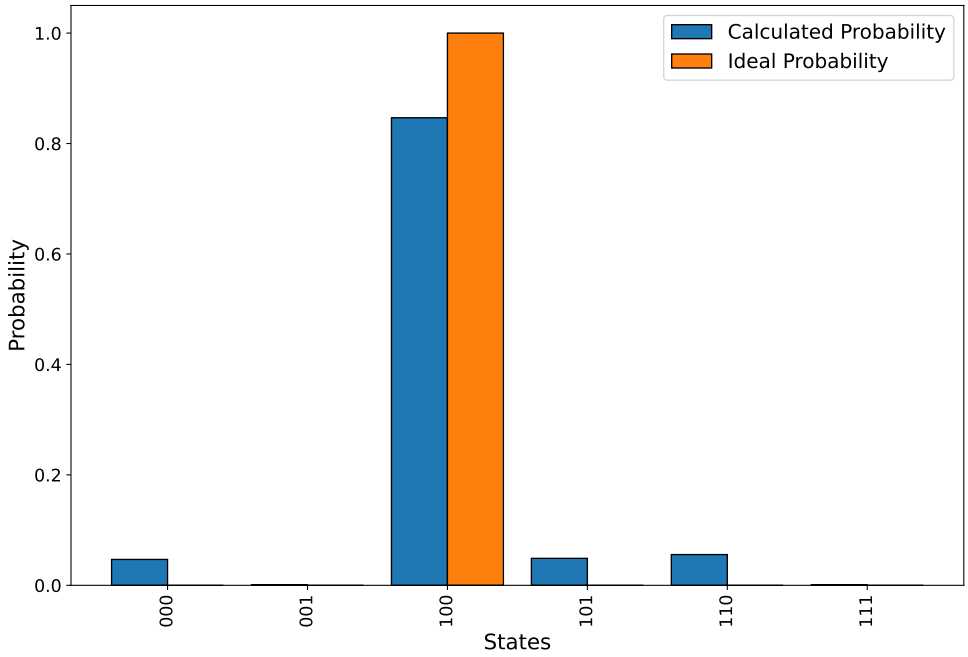

Figure 16: Impact of depolarizing error on Mermin state

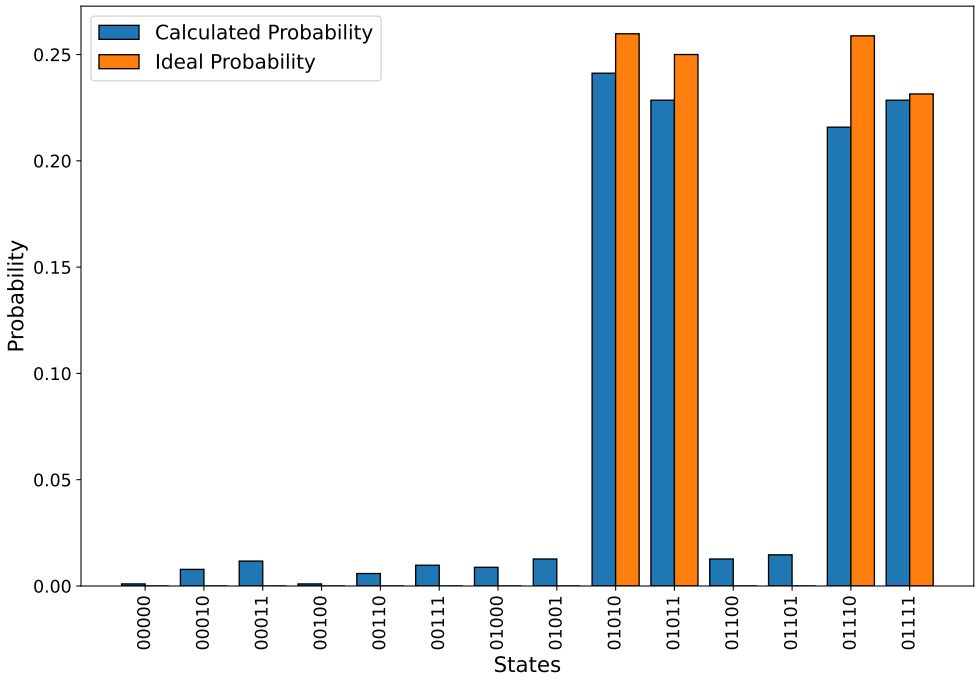

Figure 17: Impact of depolarizing error on Phase Code state

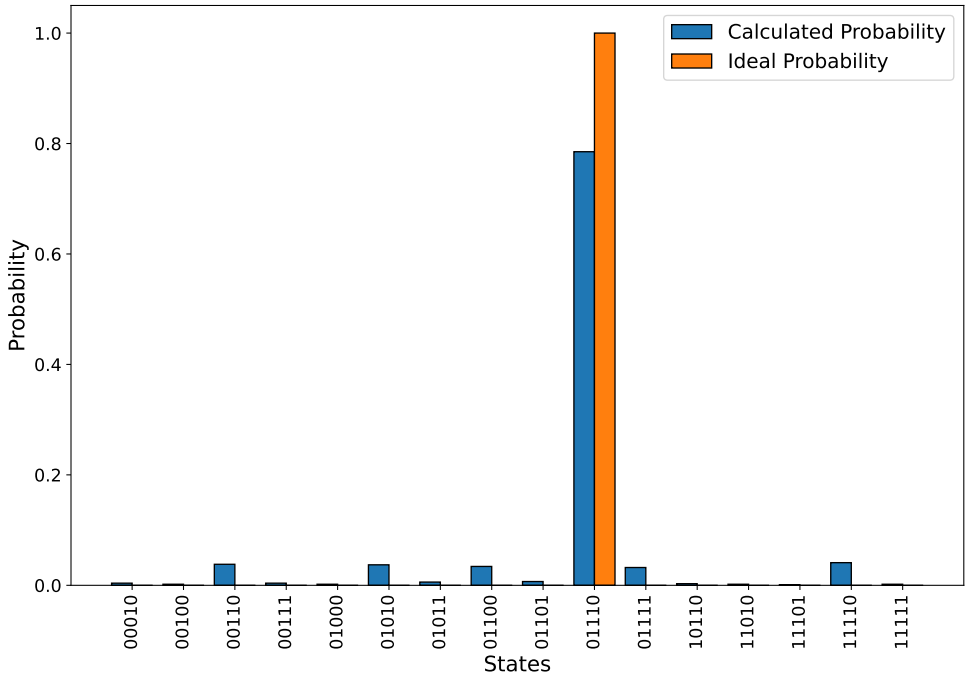

Figure 18: Impact of depolarizing error on Bit Code state

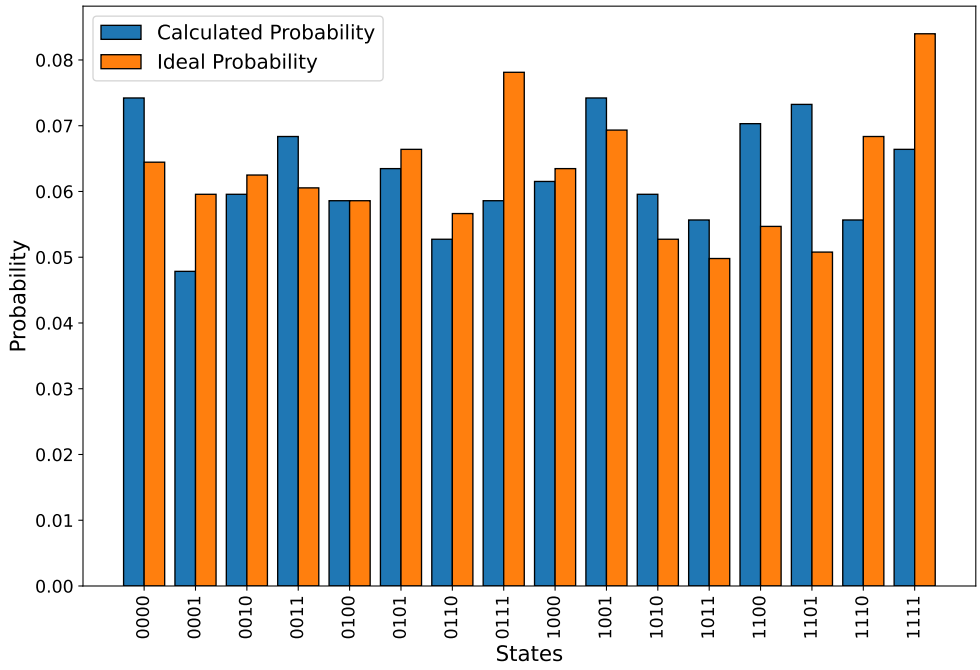

Figure 19: Impact of depolarizing error on Swap QAOA state

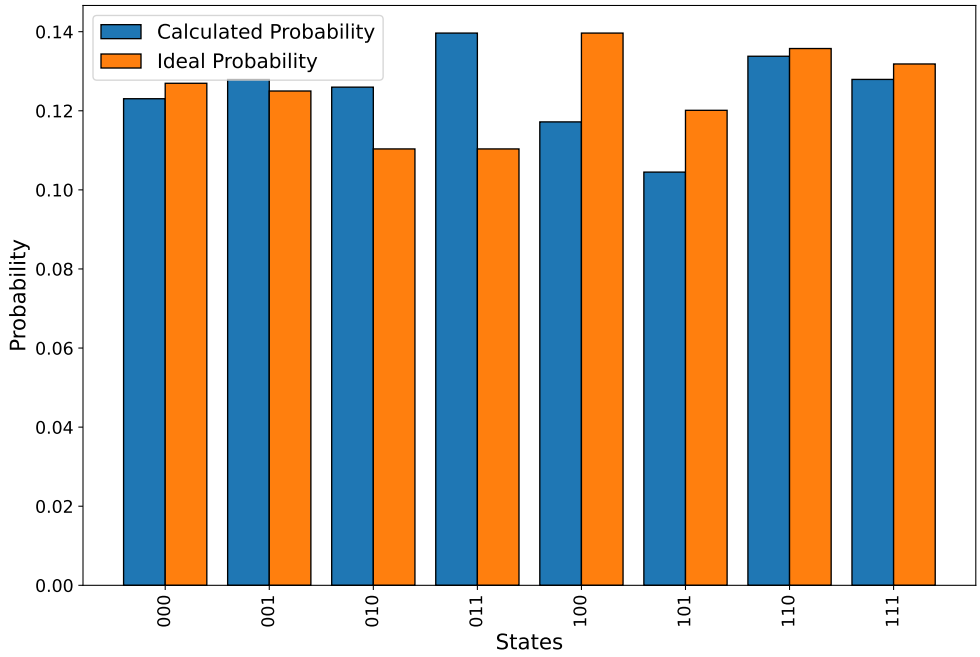

Figure 20: Impact of depolarizing error on Vanilla QAOA state

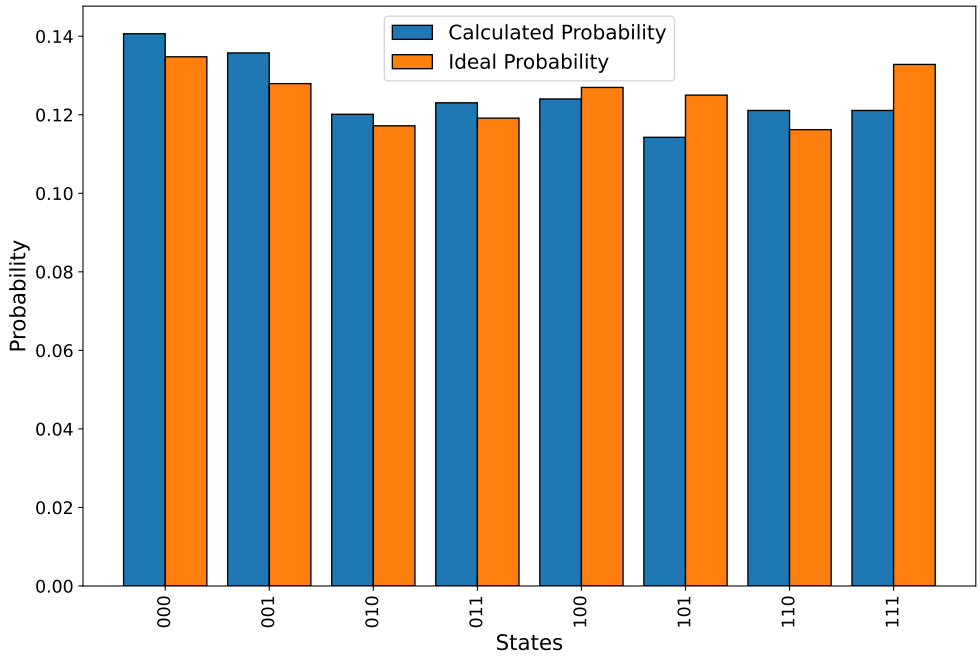

Figure 21: Impact of depolarizing error on Hamiltonian state

5.3 Thermal Noise Error

Both thermal relaxation time constant T_1 and dephasing time constant T_2 is sampled for $50\mu s$

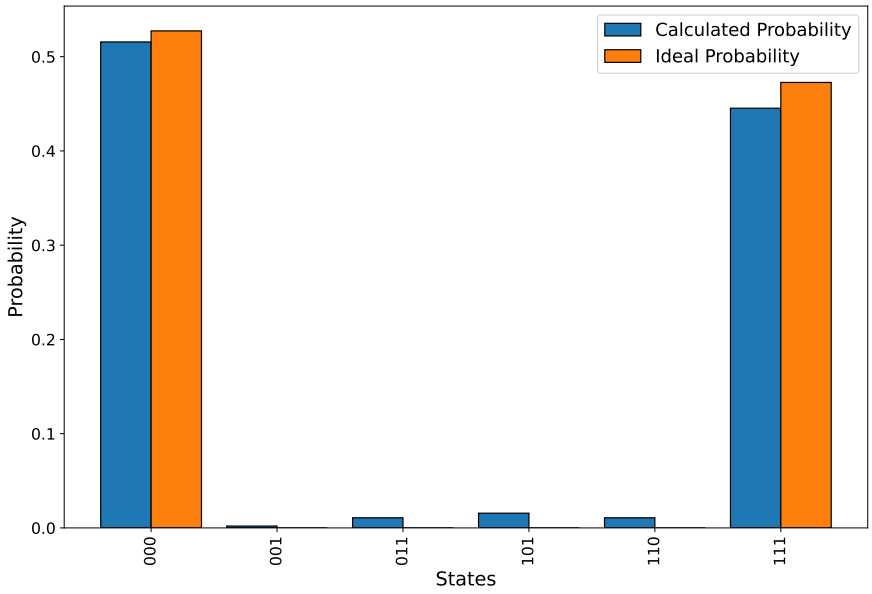

Figure 22: Impact of thermal error on GHZ state

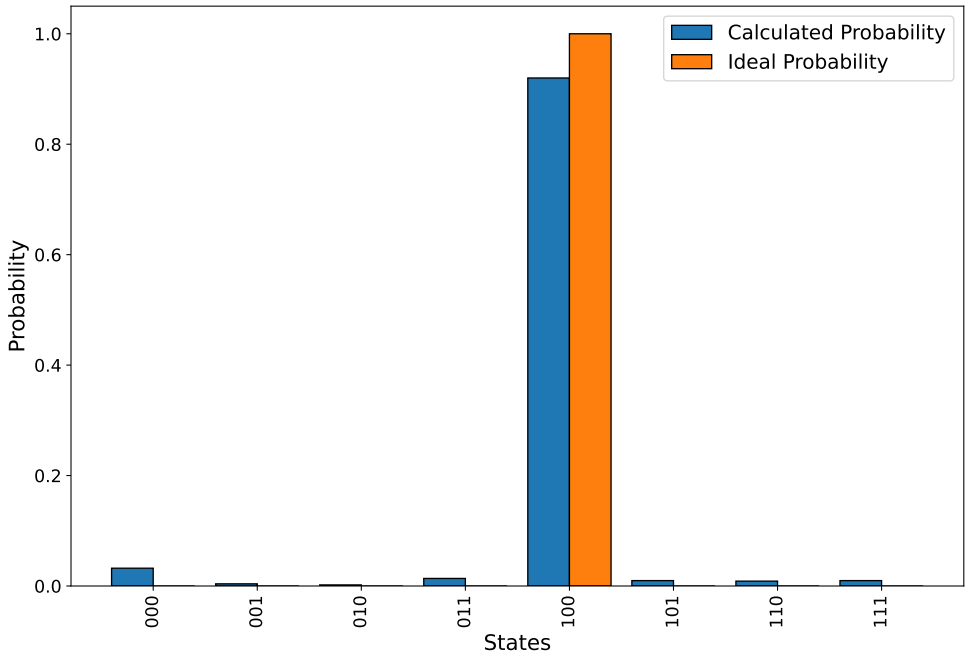

Figure 23: Impact of thermal error on Mermin state

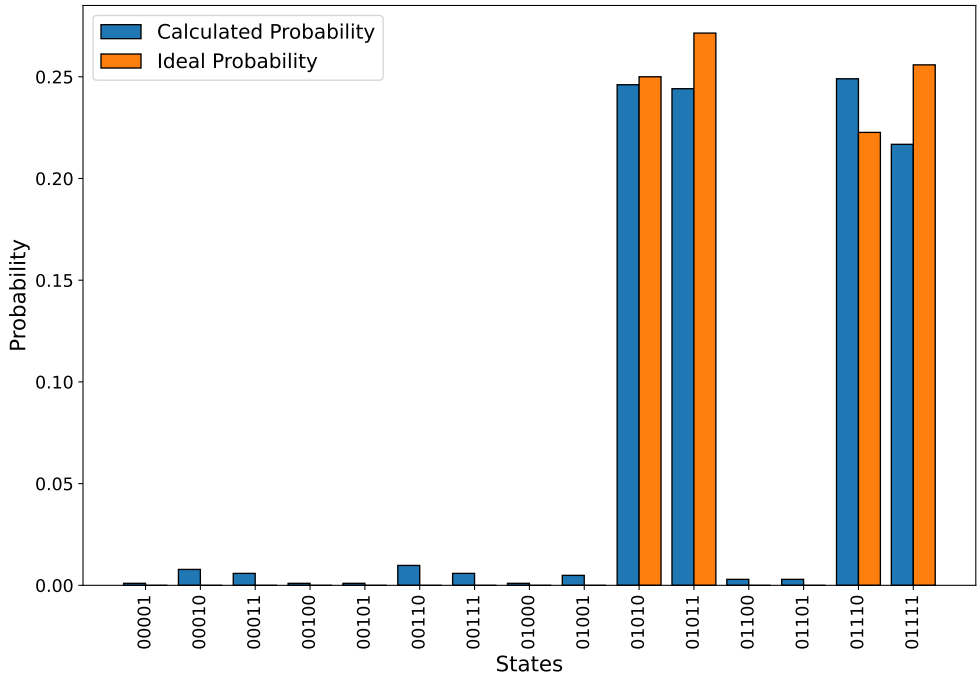

Figure 24: Impact of thermal error on Phase Code state

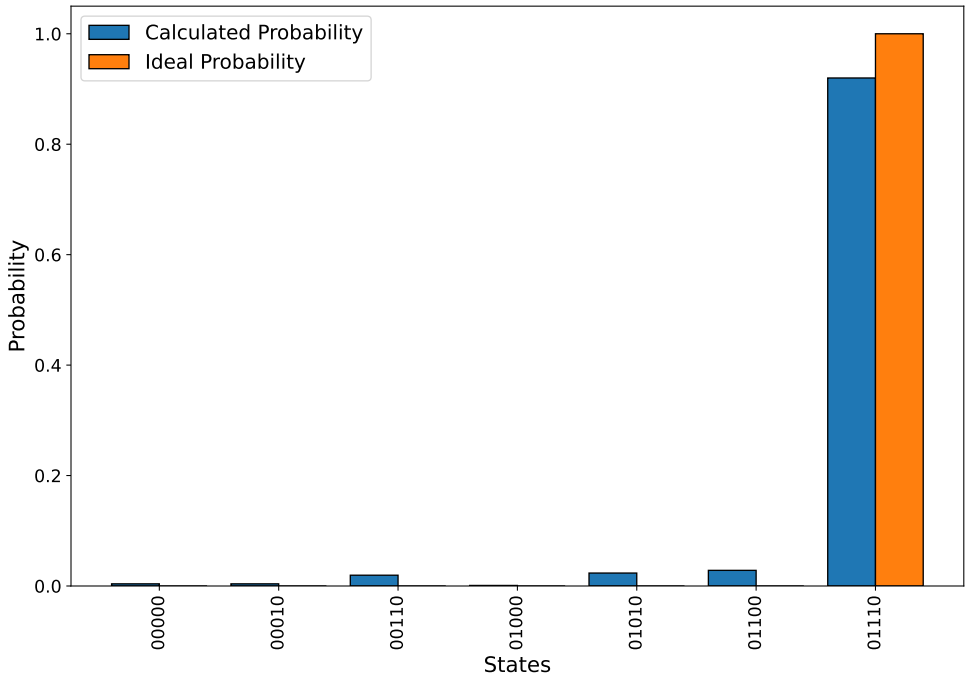

Figure 25: Impact of thermal error on Bit Code state

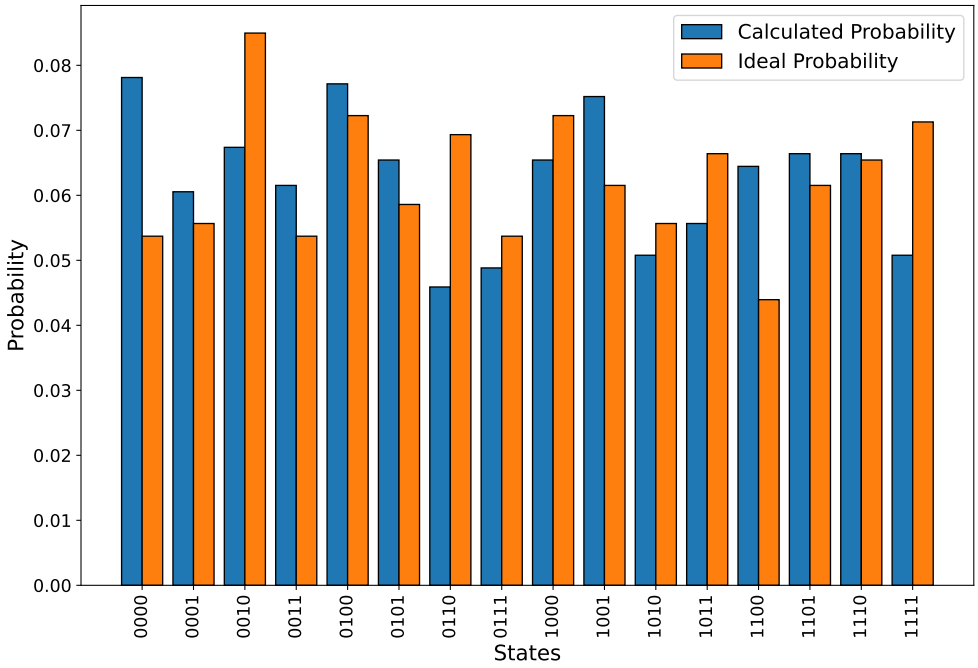

Figure 26: Impact of thermal error on Swap QAOA state

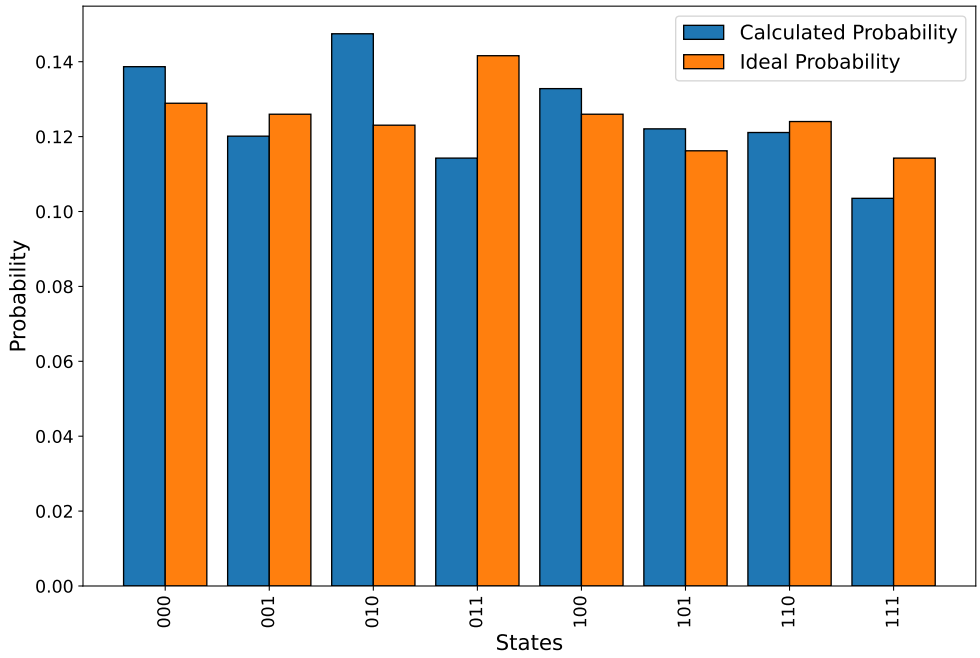

Figure 27: Impact of thermal error on Vanilla QAOA state

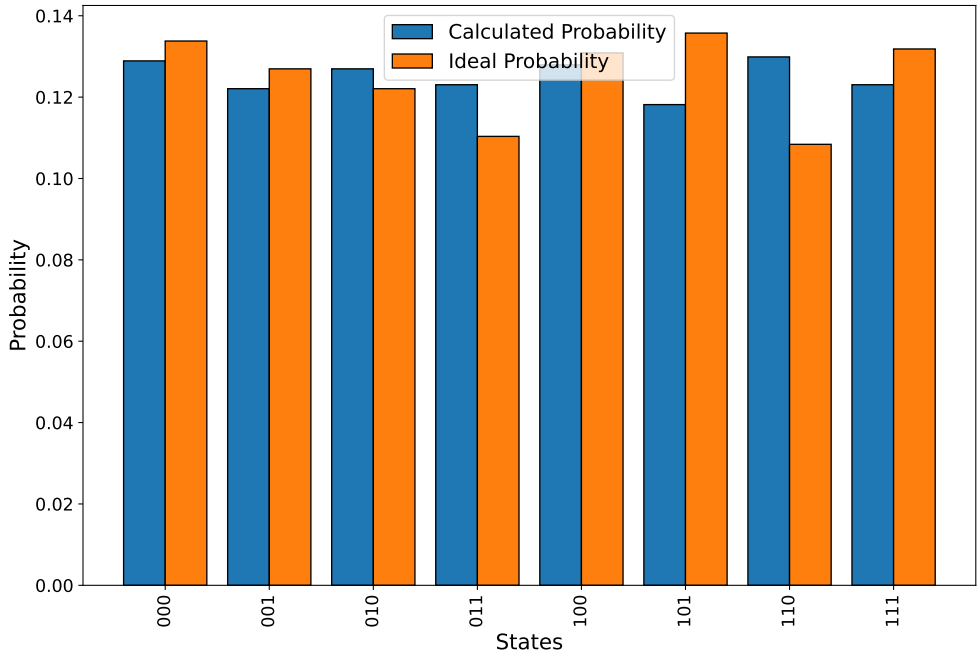

Figure 28: Impact of thermal error on Hamiltonian state

5.3.1 Results on Real Devices

We also made a comparison of our noise model against all open access quantum processors available by IBM Quantum. Processor specified *coupling map* is also considered so that full distance matrix of the graphs can be utilised. There are three legends in this section histogram plots: *Experimental Probability*: Output for IBM Quantum Processor, *Simulated Probability*: In this case, we modeled all three errors in a whole and *Ideal Probability*: Simulation on *AerSimulator*.

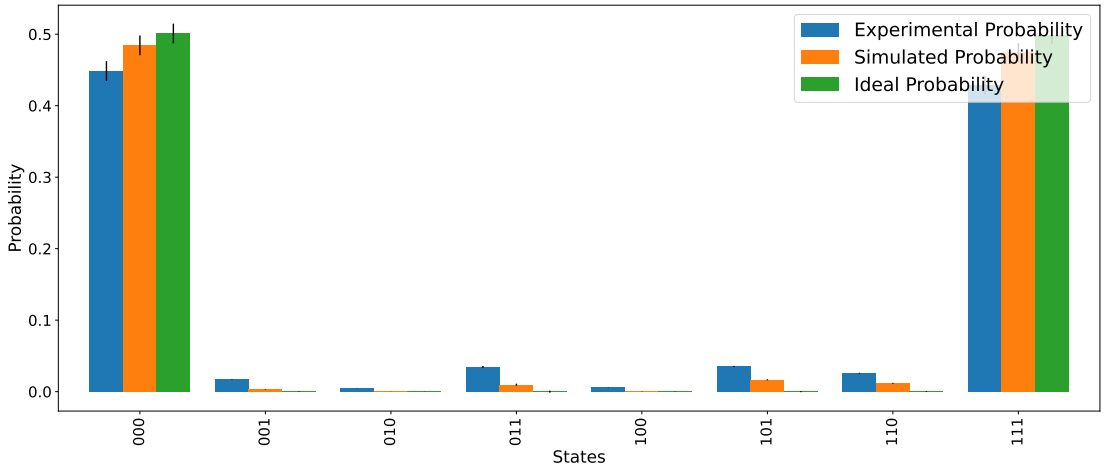

Figure 29: GHZ circuit on Nairobi backend

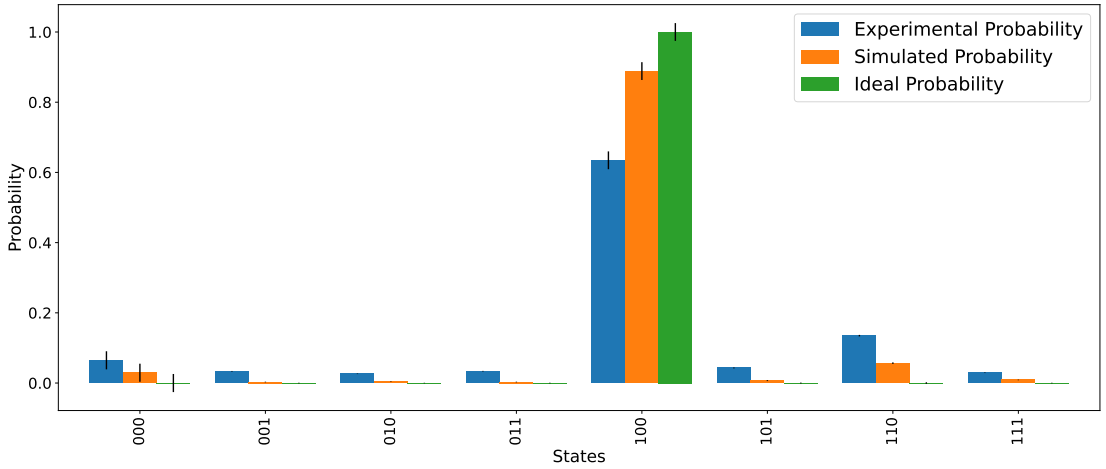

Figure 30: Mermin Bell circuit on Nairobi backend

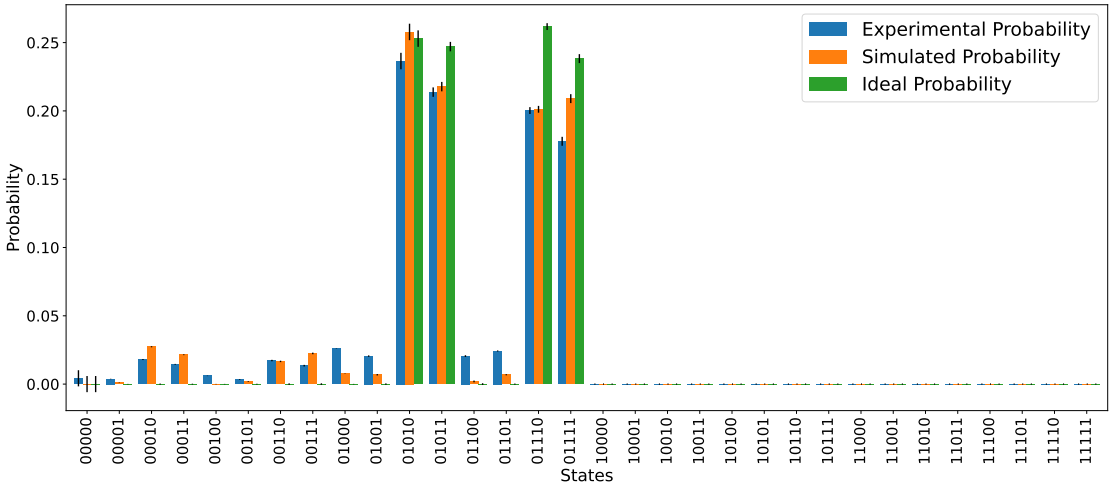

Figure 31: Phase circuit on Nairobi backend

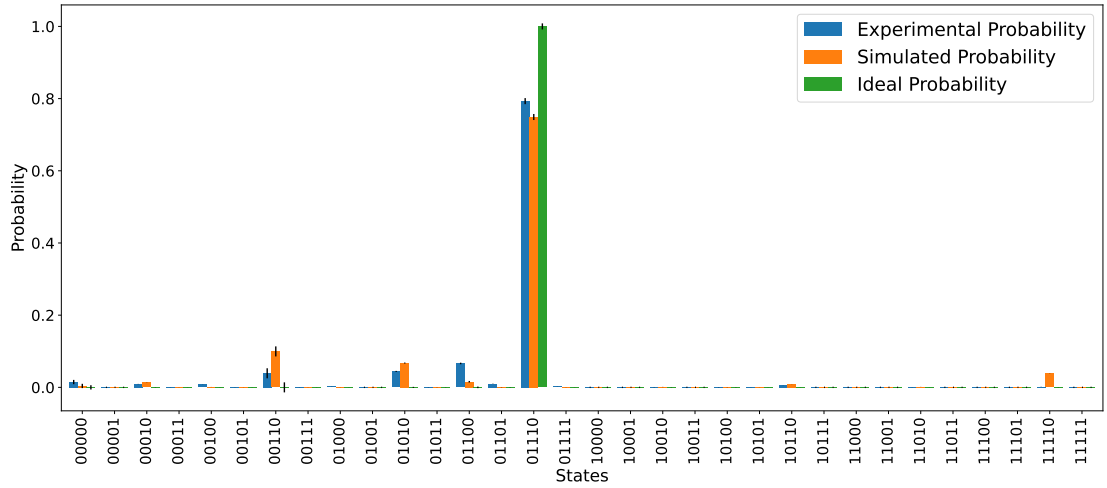

Figure 32: Bit circuit on Nairobi backend

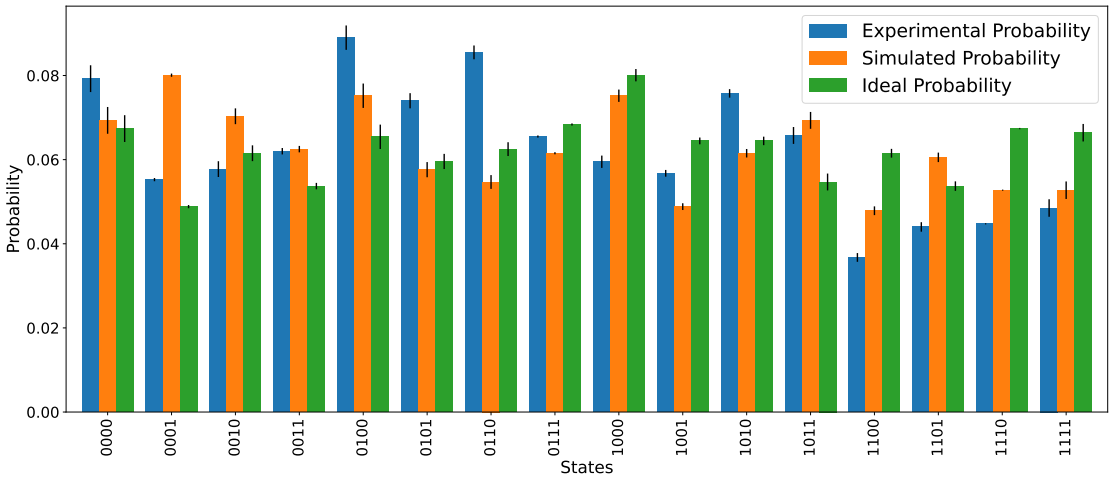

Figure 33: Swap QAOA circuit on Nairobi backend

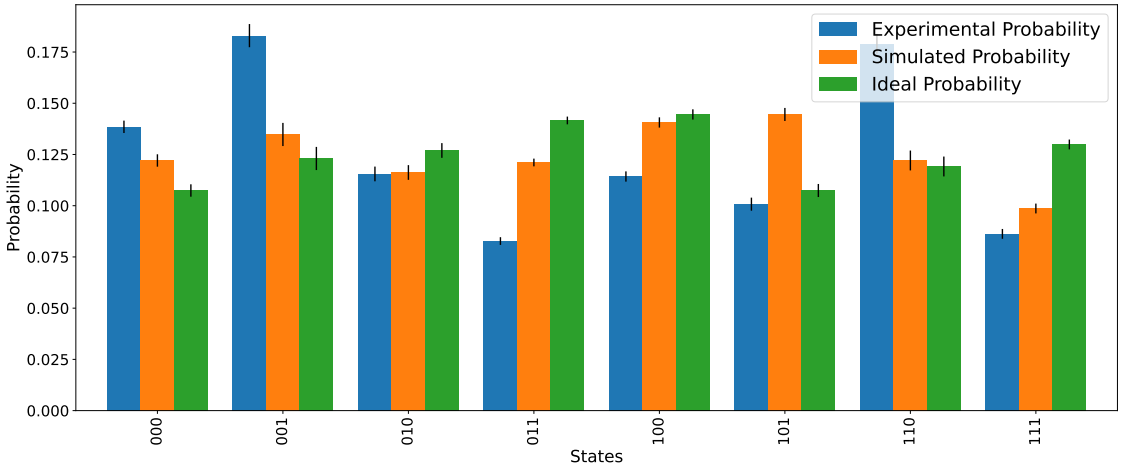

Figure 34: Vanilla QAOA circuit on Nairobi backend

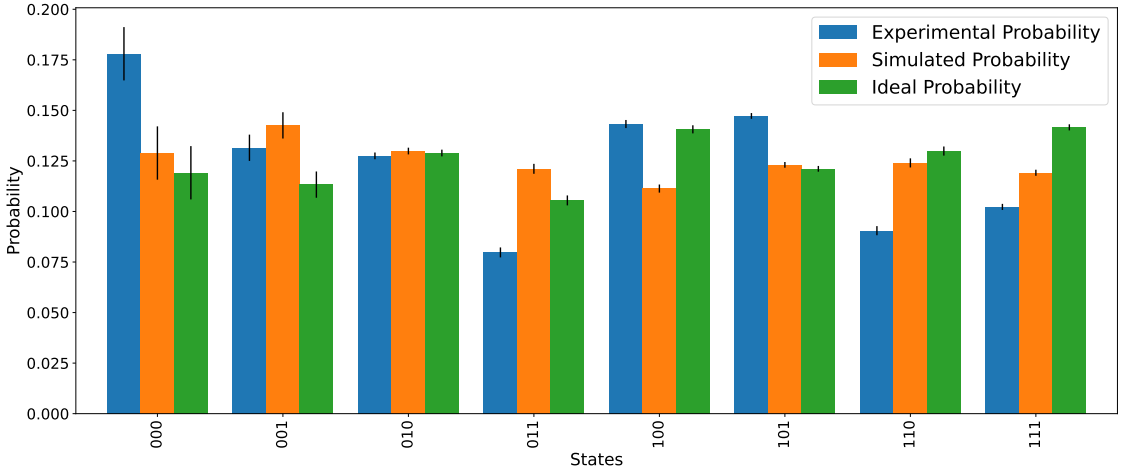

Figure 35: Hamiltonian circuit on Nairobi backend

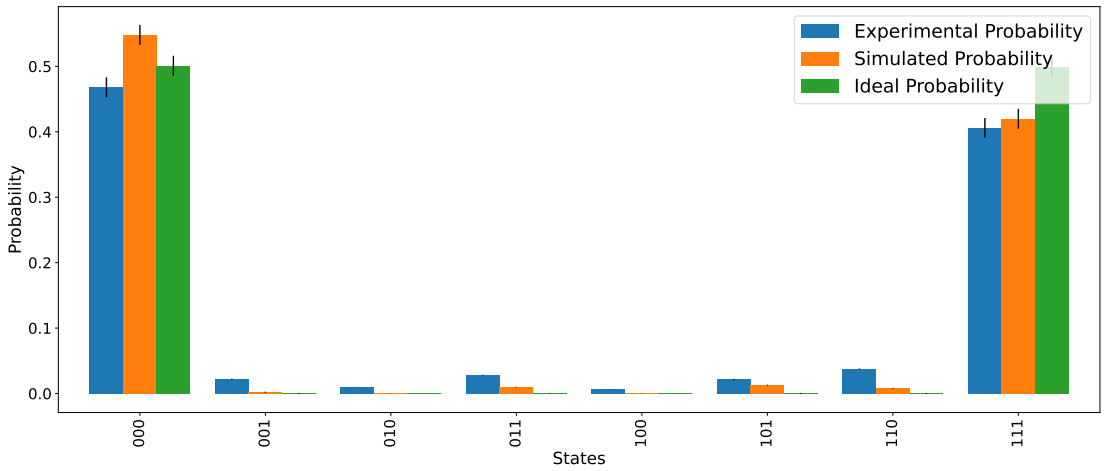

Figure 36: GHZ circuit on Belem backend

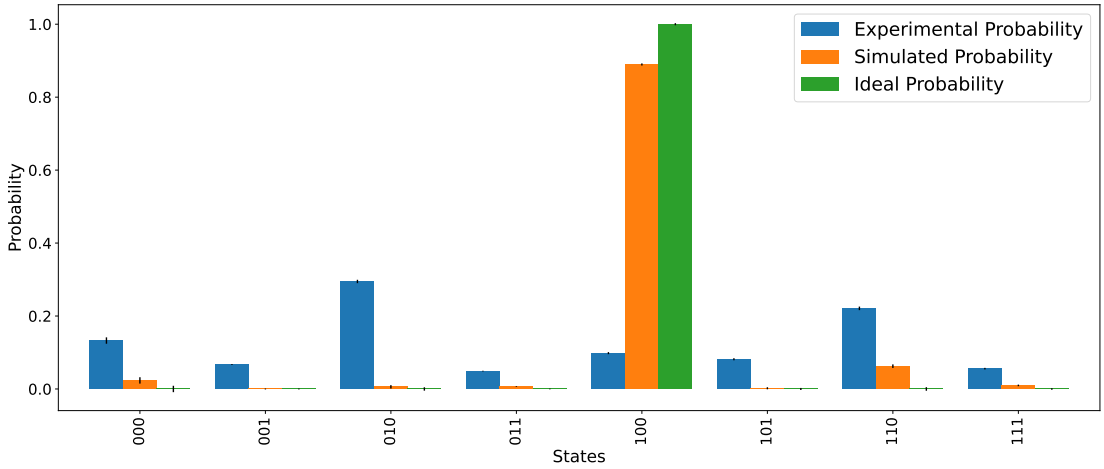

Figure 37: Mermin Bell circuit on Belem backend

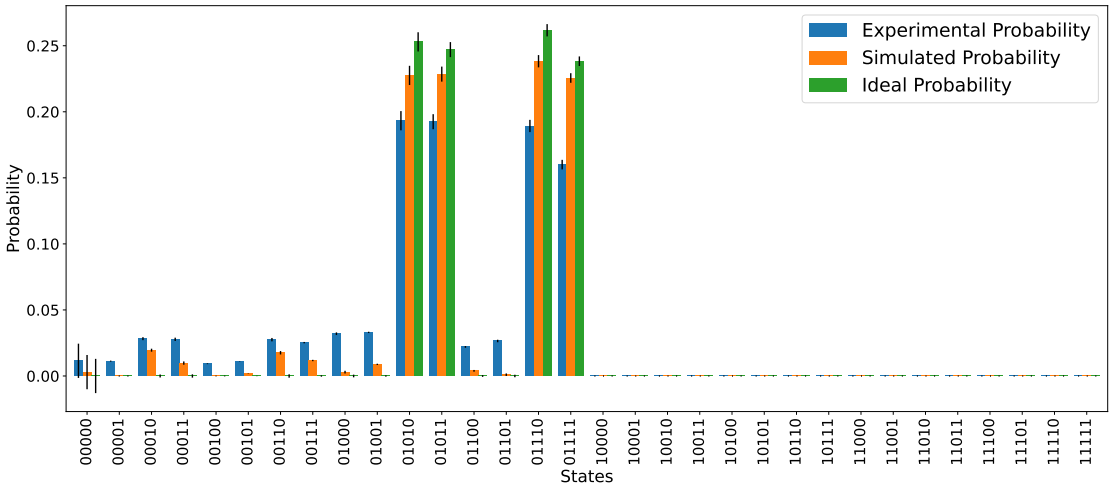

Figure 38: Phase circuit on Belem backend

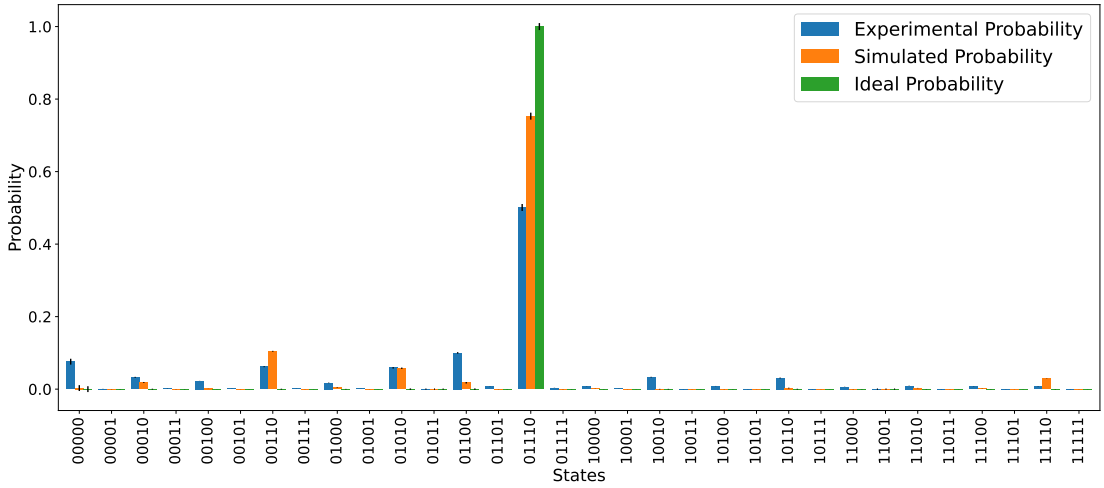

Figure 39: Bit circuit on Belem backend

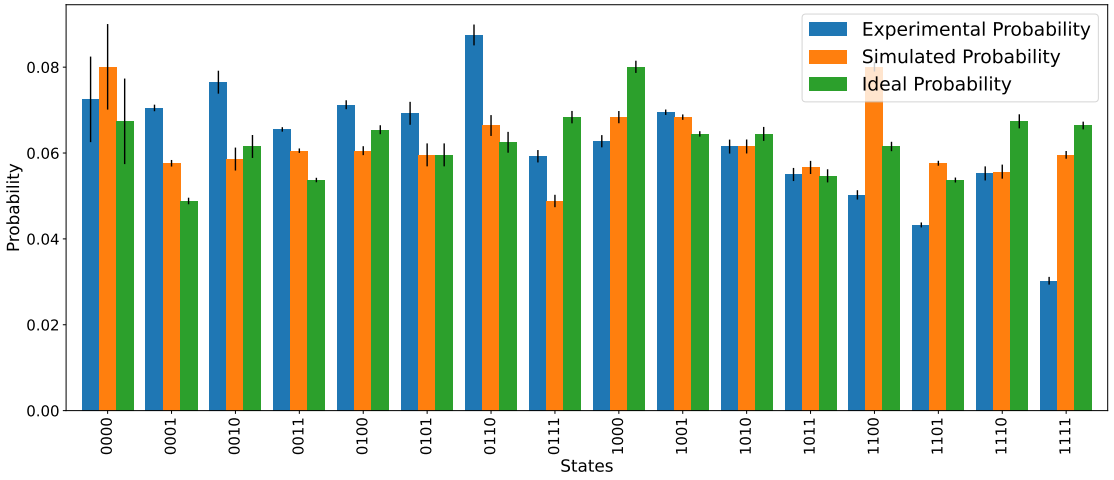

Figure 40: Swap QAOA circuit on Belem backend

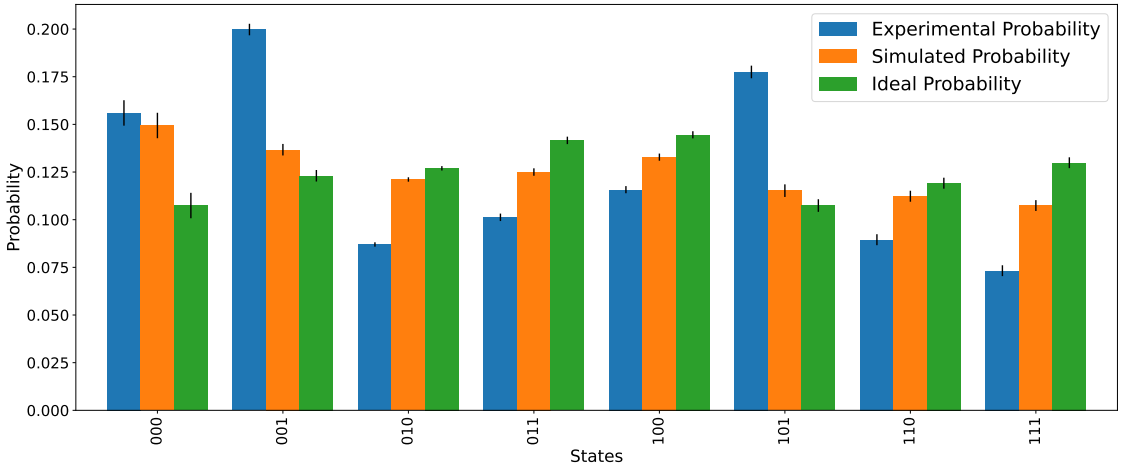

Figure 41: Vanilla QAOA circuit on Belem backend

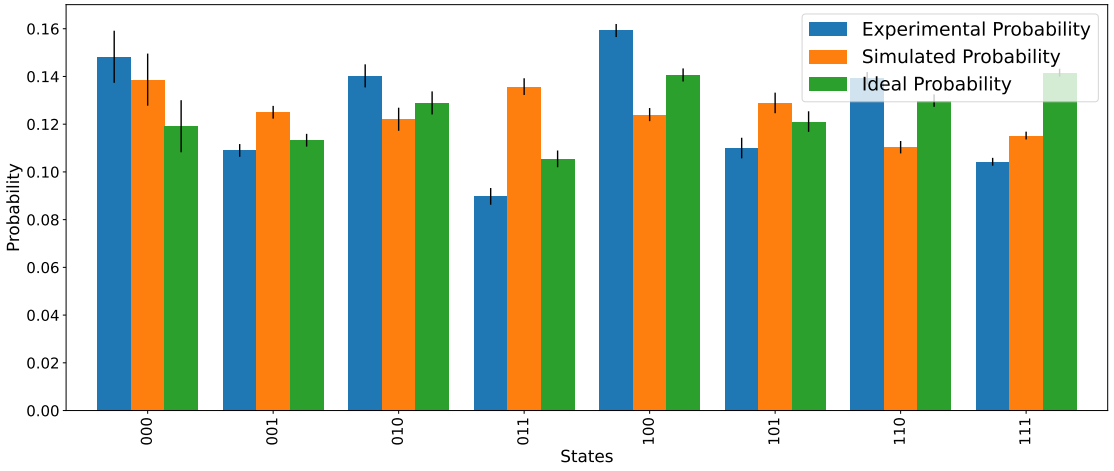

Figure 42: Hamiltonian circuit on Belem backend

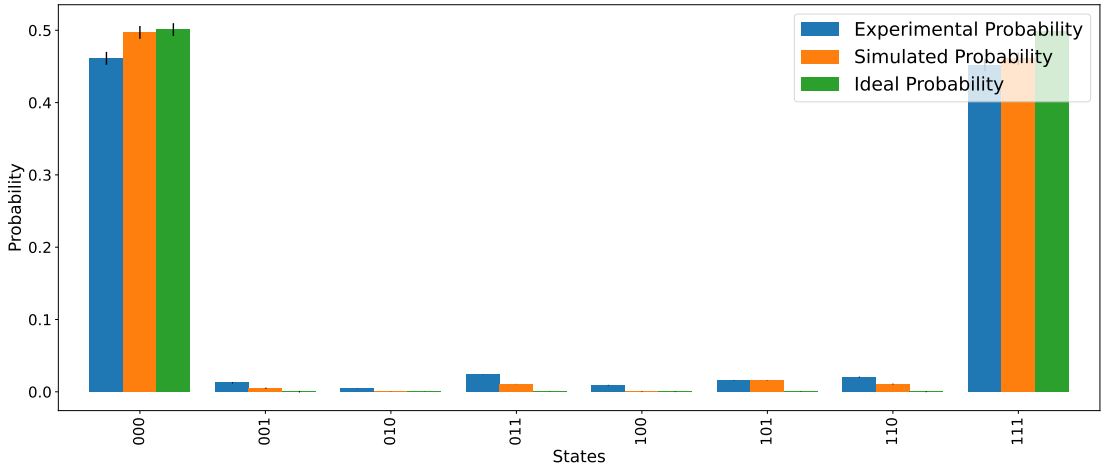

Figure 43: GHZ circuit on Lima backend

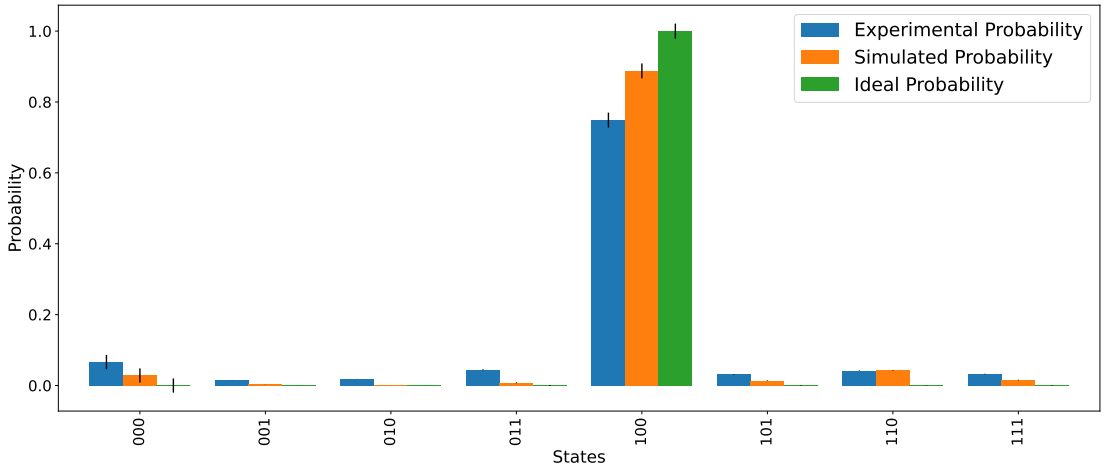

Figure 44: Mermin Bell circuit on Lima backend

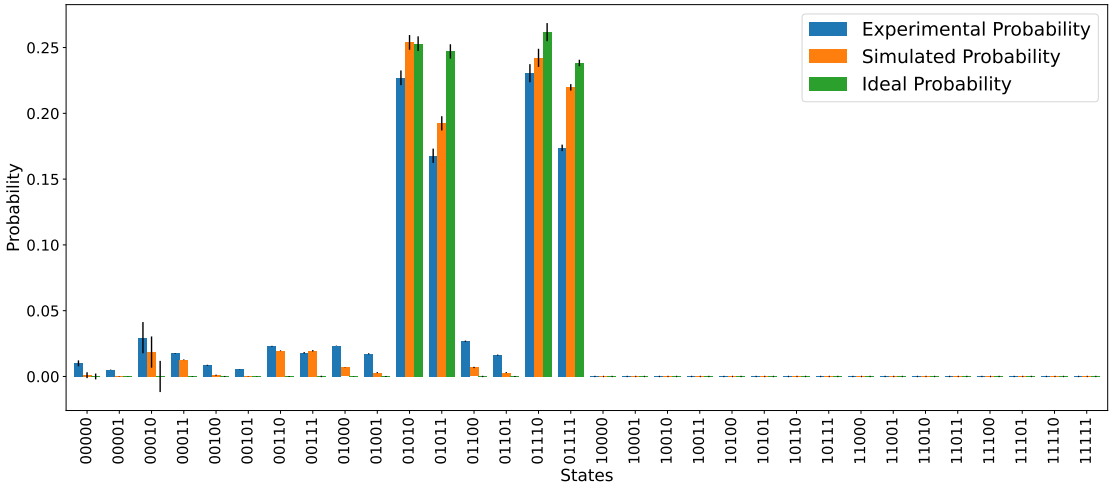

Figure 45: Phase circuit on Lima backend

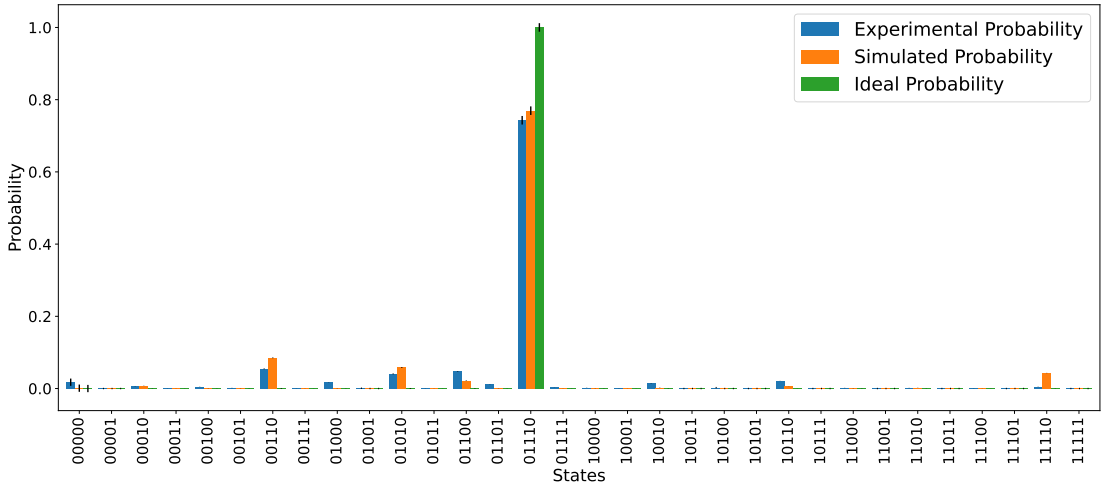

Figure 46: Bit circuit on Lima backend

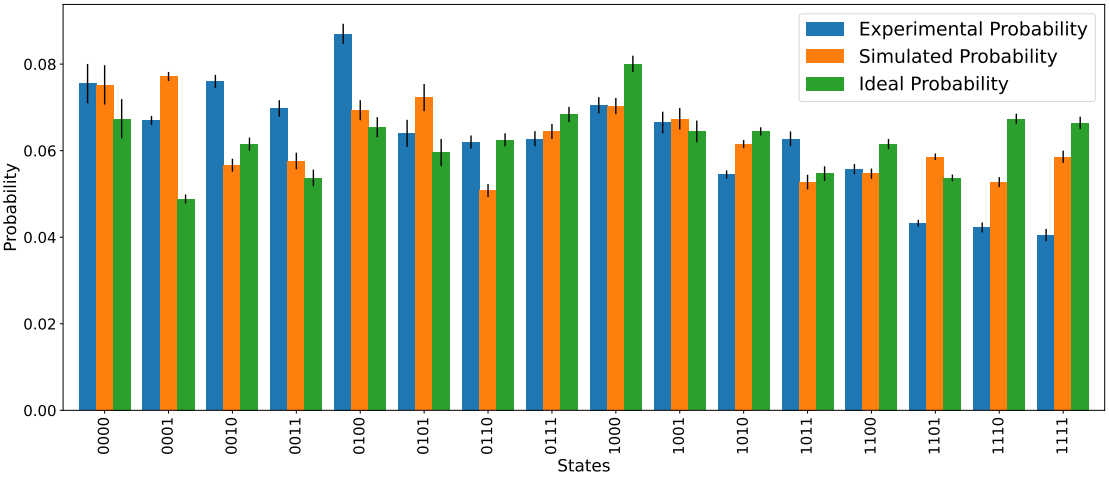

Figure 47: Swap QAOA circuit on Lima backend

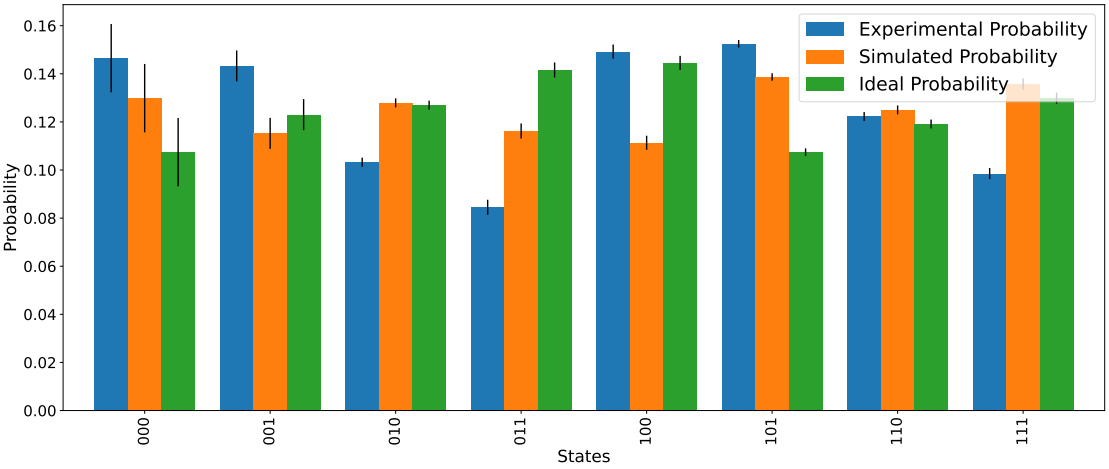

Figure 48: Vanilla QAOA circuit on Lima backend

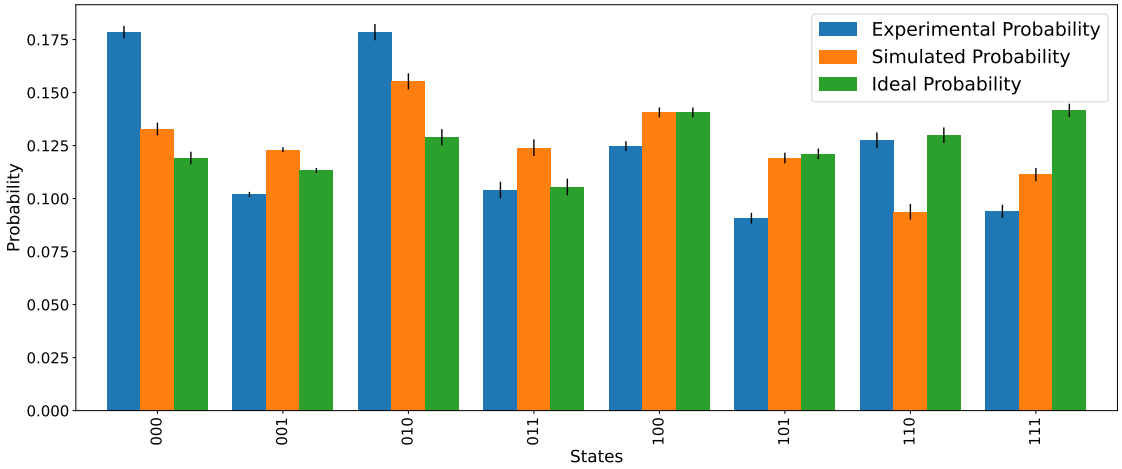

Figure 49: Hamiltonian circuit on Lima backend

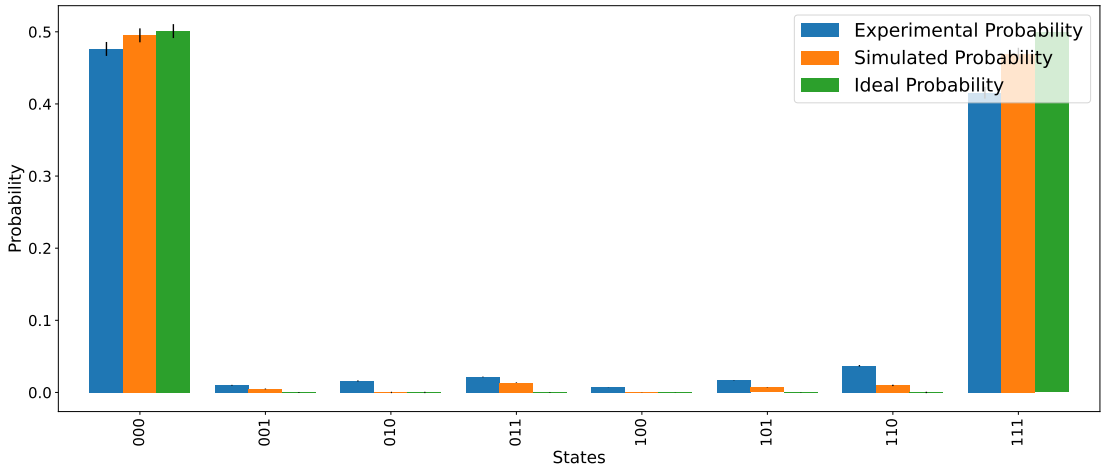

Figure 50: GHZ circuit on Manila backend

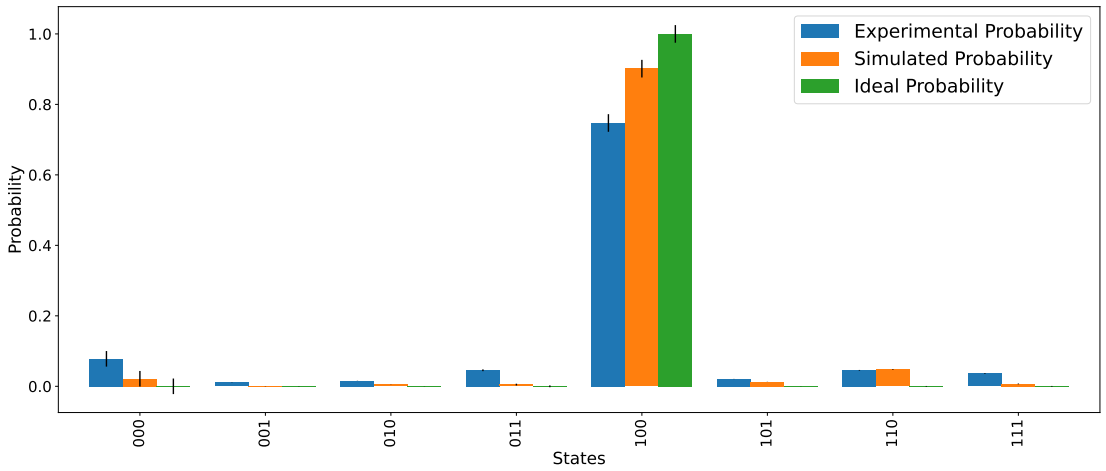

Figure 51: Mermin Bell circuit on Manila backend

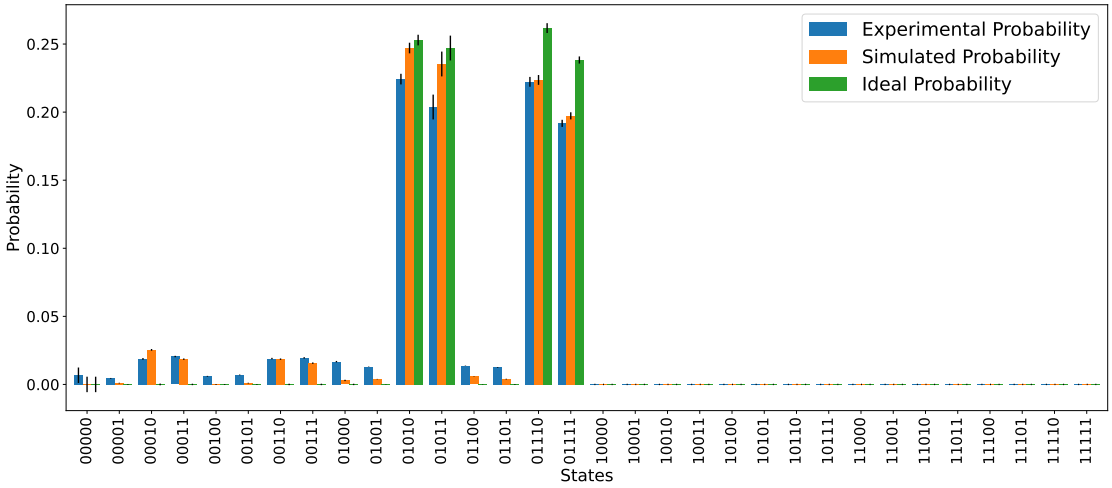

Figure 52: Phase circuit on Manila backend

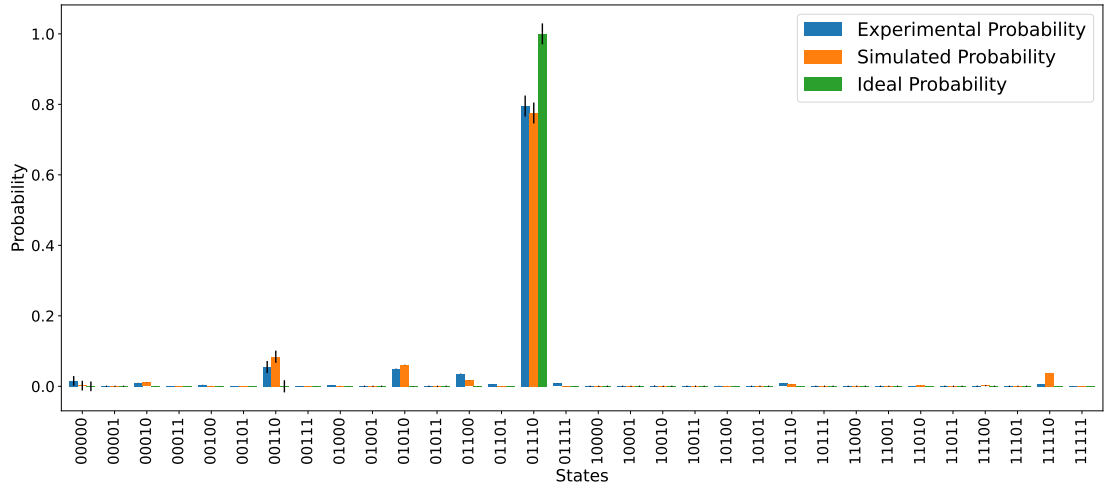

Figure 53: Bit circuit on Manila backend

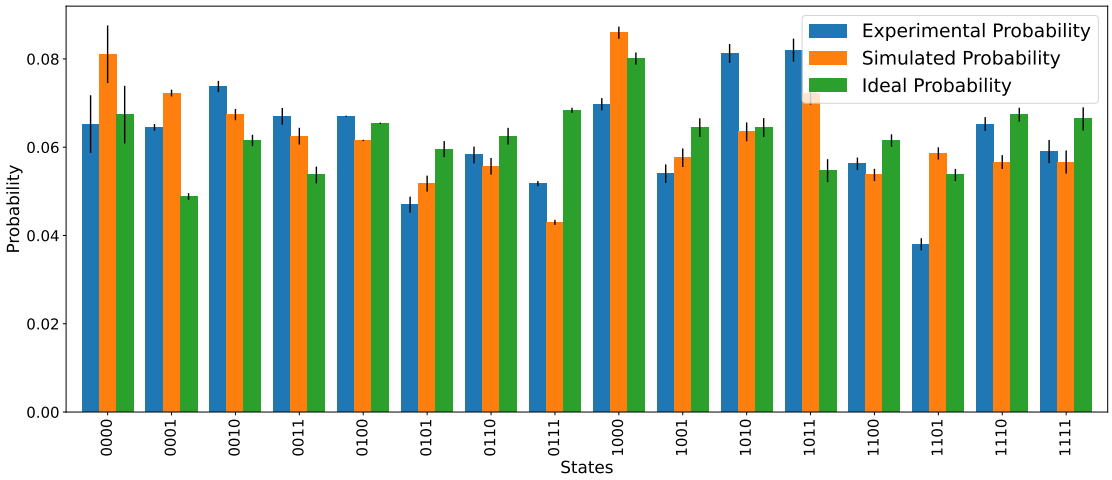

Figure 54: Swap QAOA circuit on Manila backend

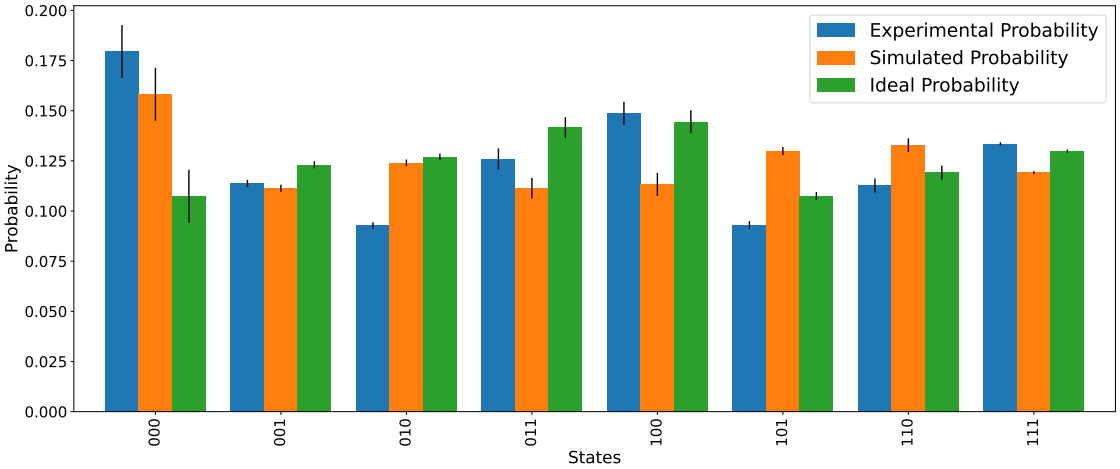

Figure 55: Vanilla QAOA circuit on Manila backend

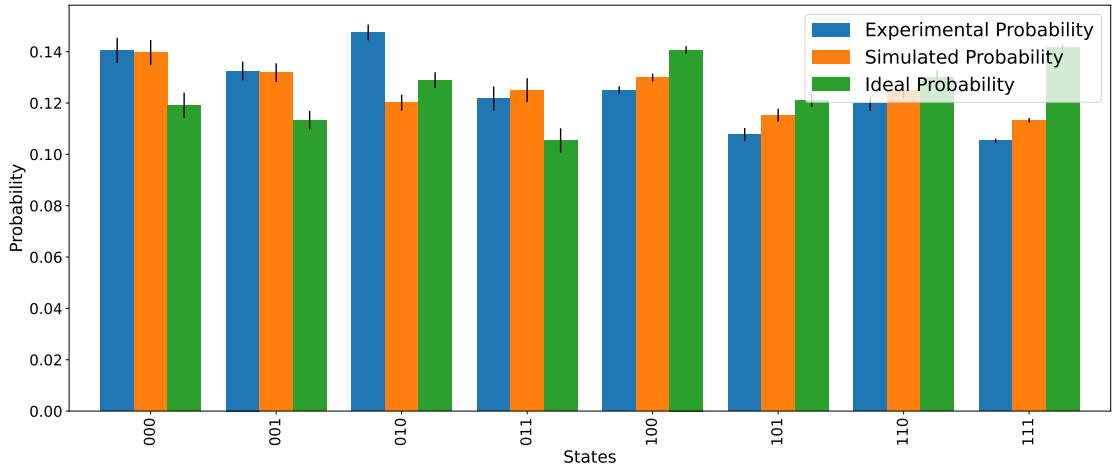

Figure 56: Hamiltonian circuit on Manila backend

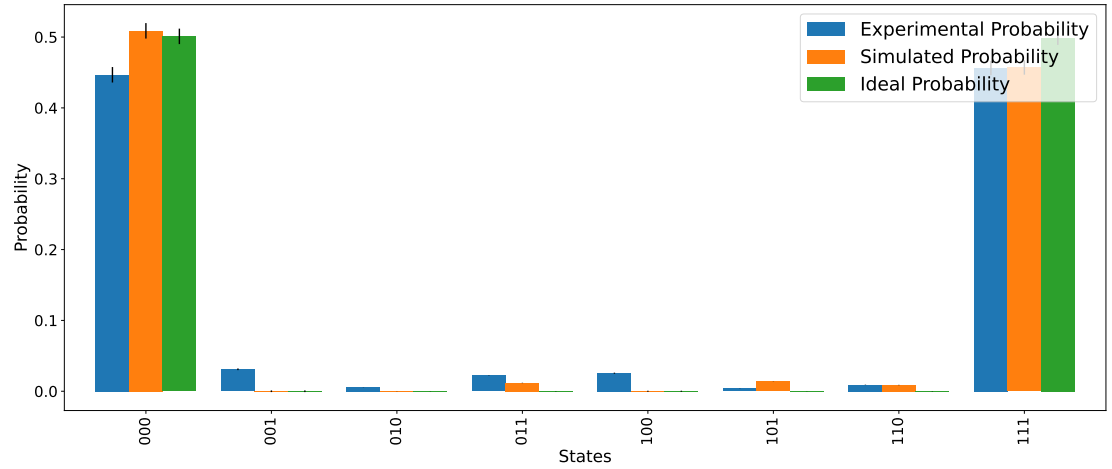

Figure 57: GHZ circuit on Oslo backend

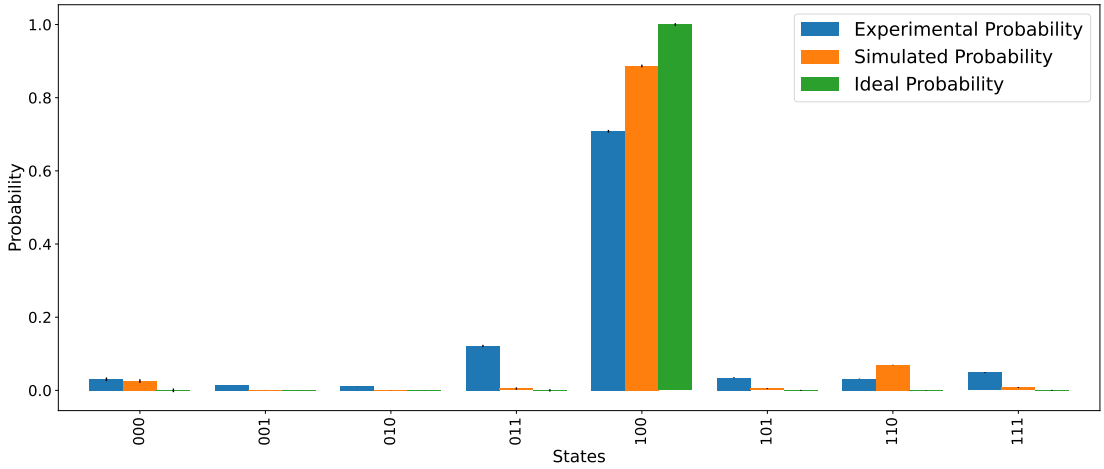

Figure 58: Mermin Bell circuit on Oslo backend

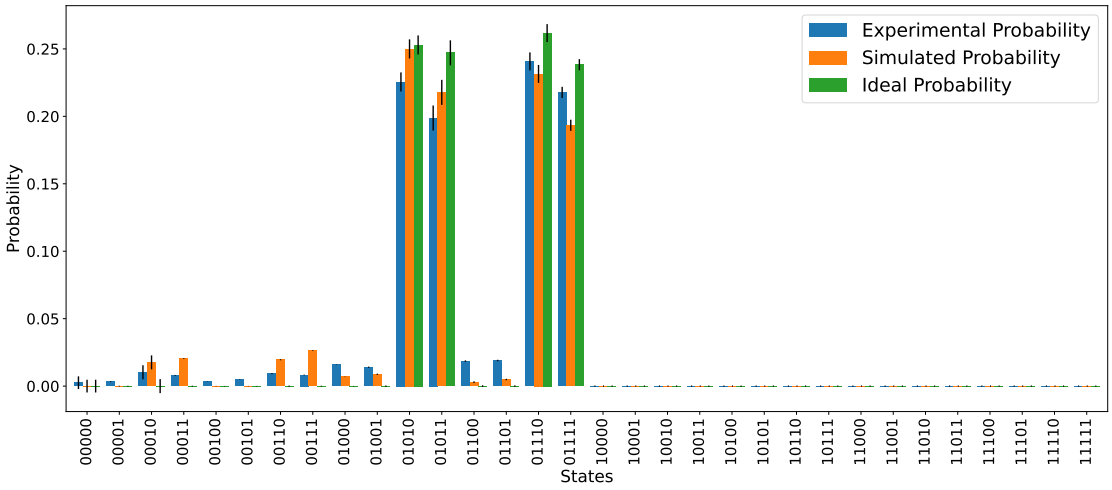

Figure 59: Phase circuit on Oslo backend

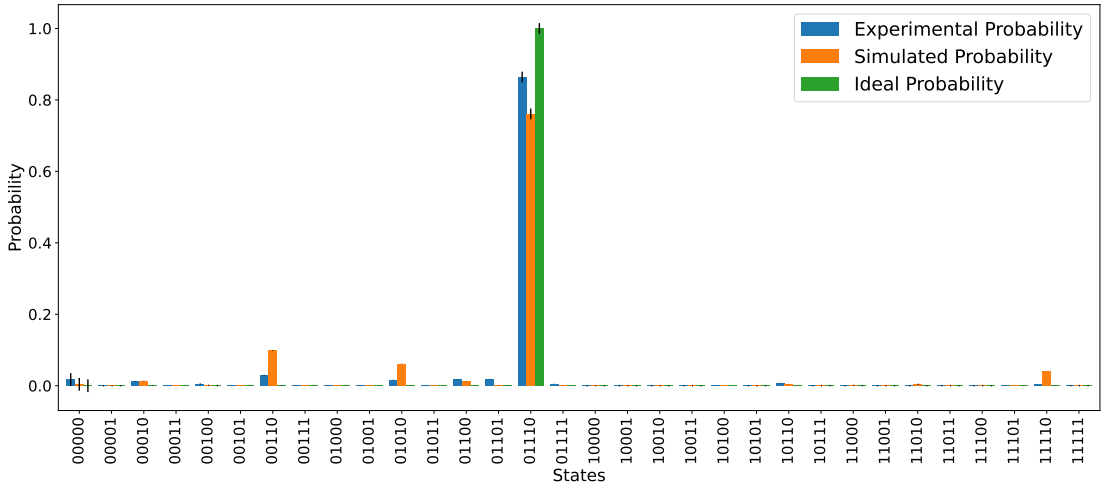

Figure 60: Bit circuit on Oslo backend

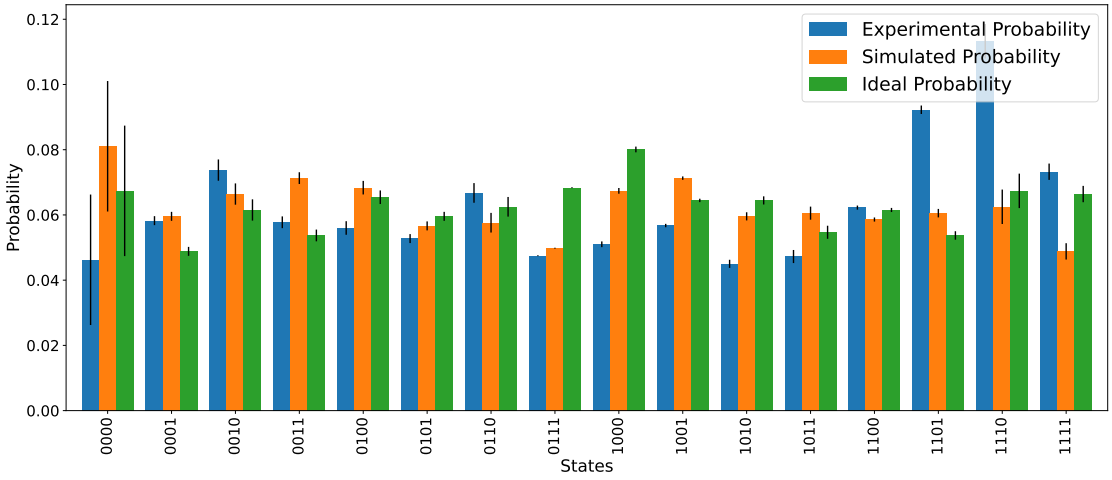

Figure 61: Swap QAOA circuit on Oslo backend

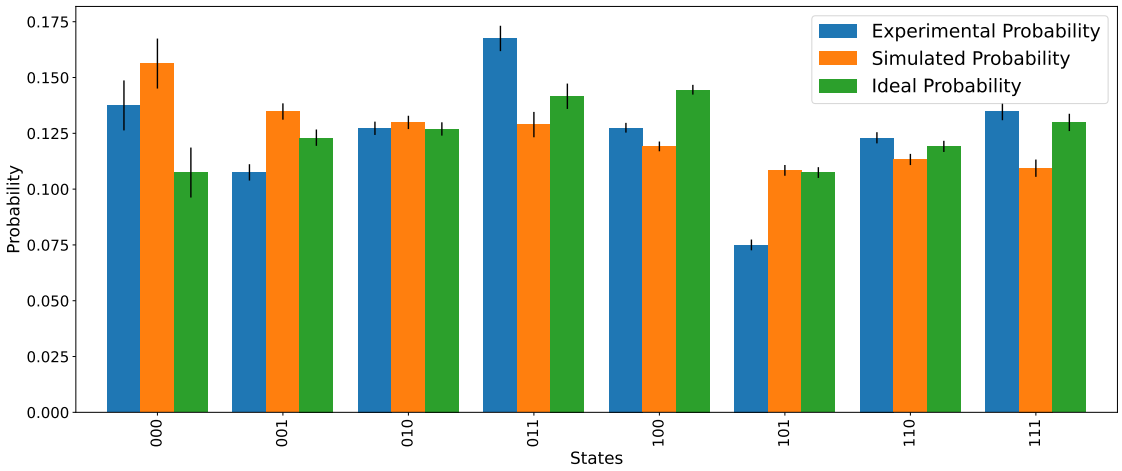

Figure 62: Vanilla QAOA circuit on Oslo backend

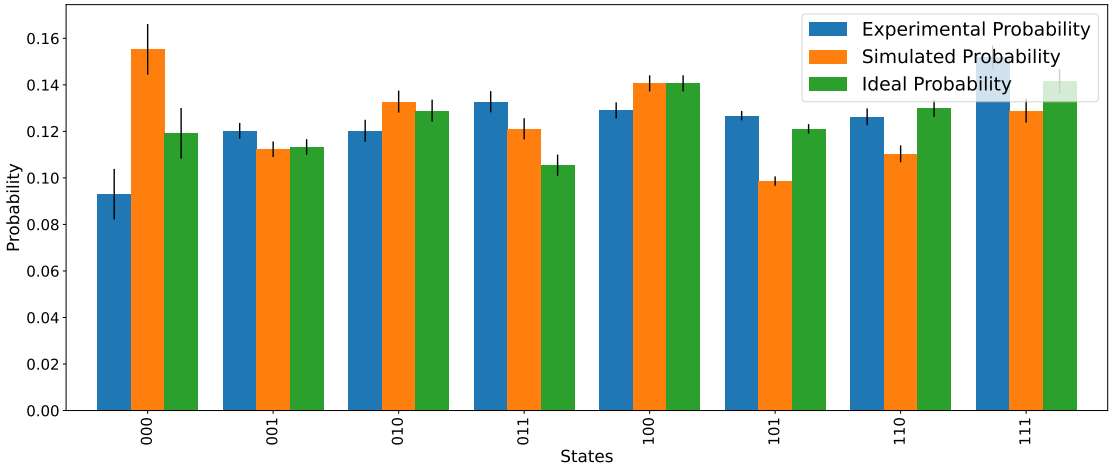

Figure 63: Hamiltonian circuit on Oslo backend

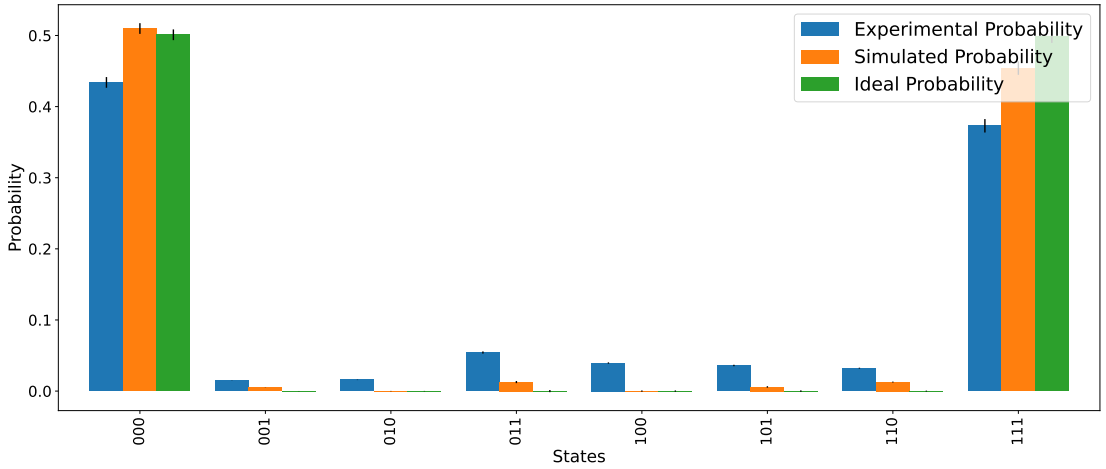

Figure 64: GHZ circuit on Quito backend

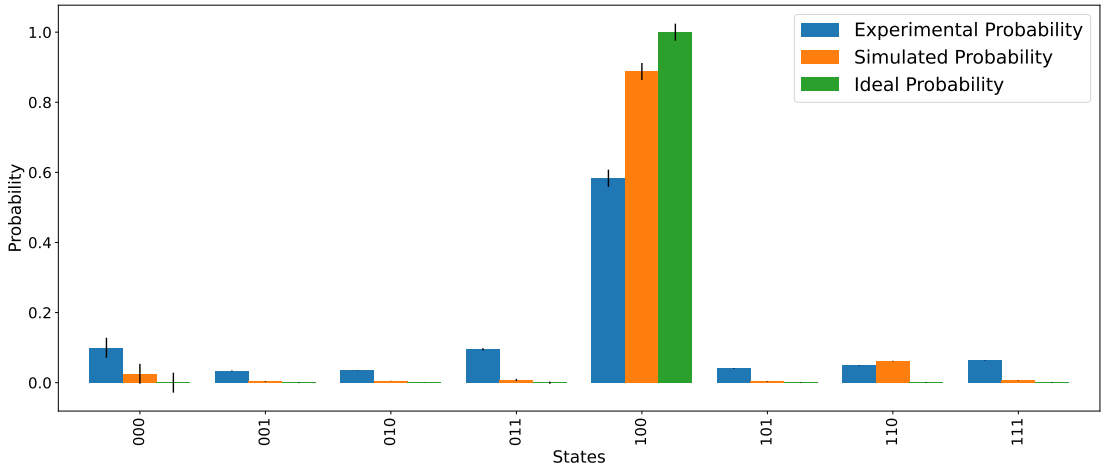

Figure 65: Mermin Bell circuit on Quito backend

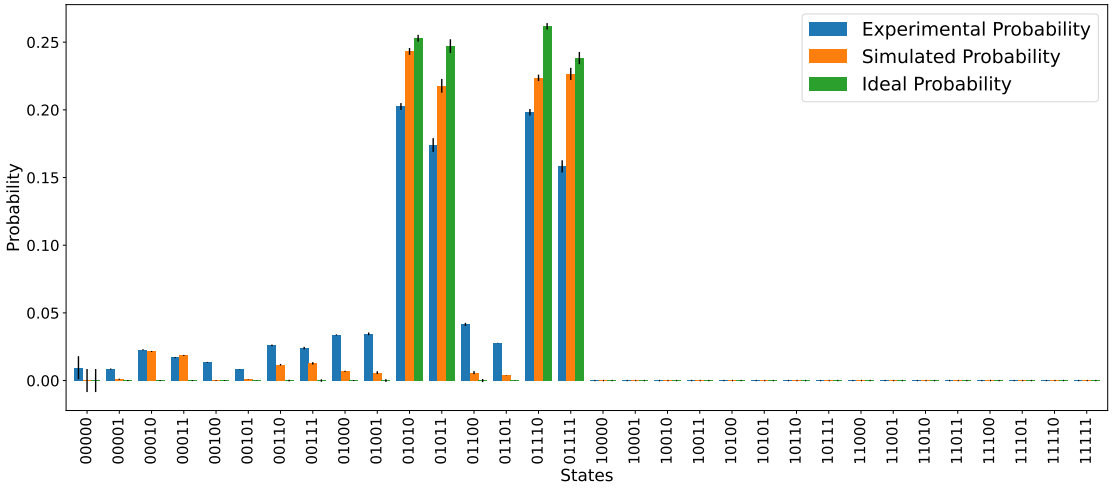

Figure 66: Phase circuit on Quito backend

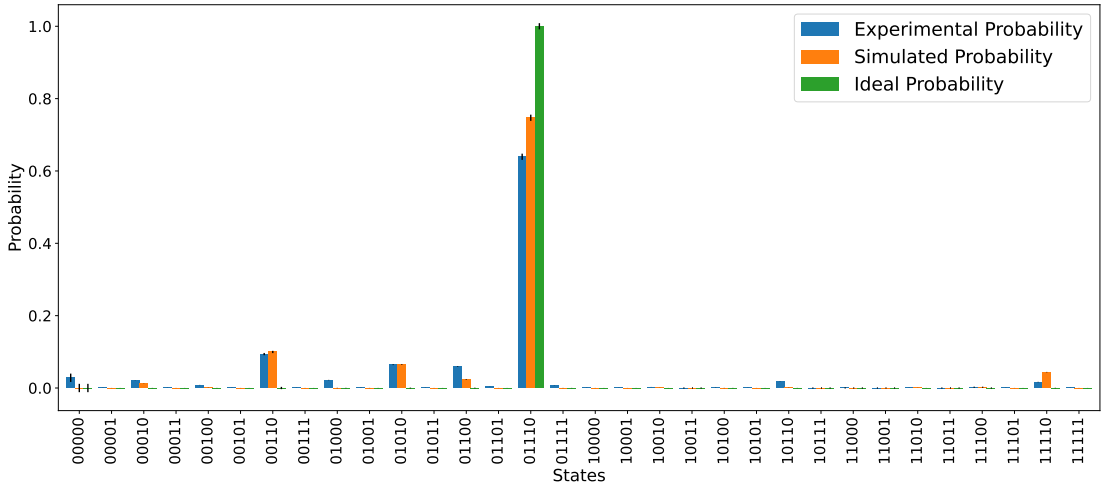

Figure 67: Bit circuit on Quito backend

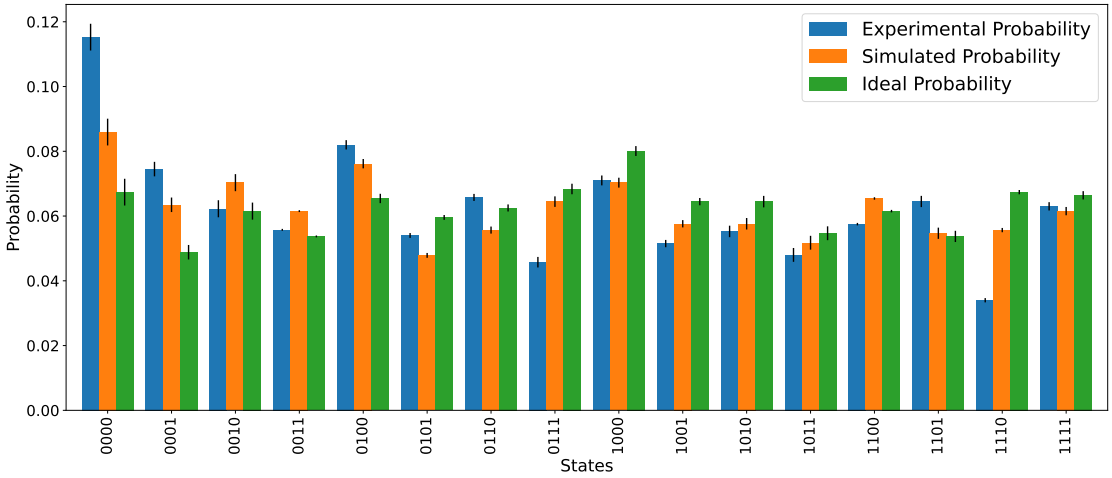

Figure 68: Swap QAOA circuit on Quito backend

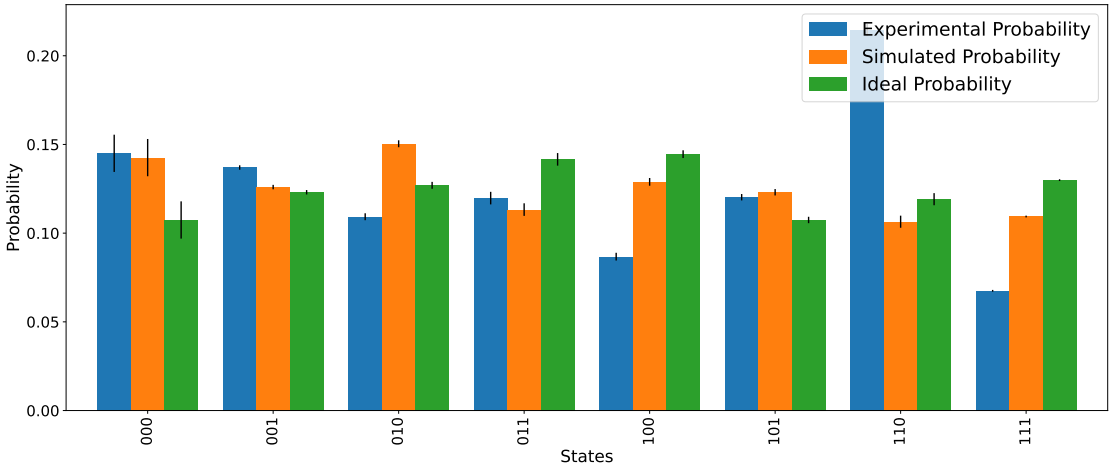

Figure 69: Vanilla QAOA circuit on Quito backend

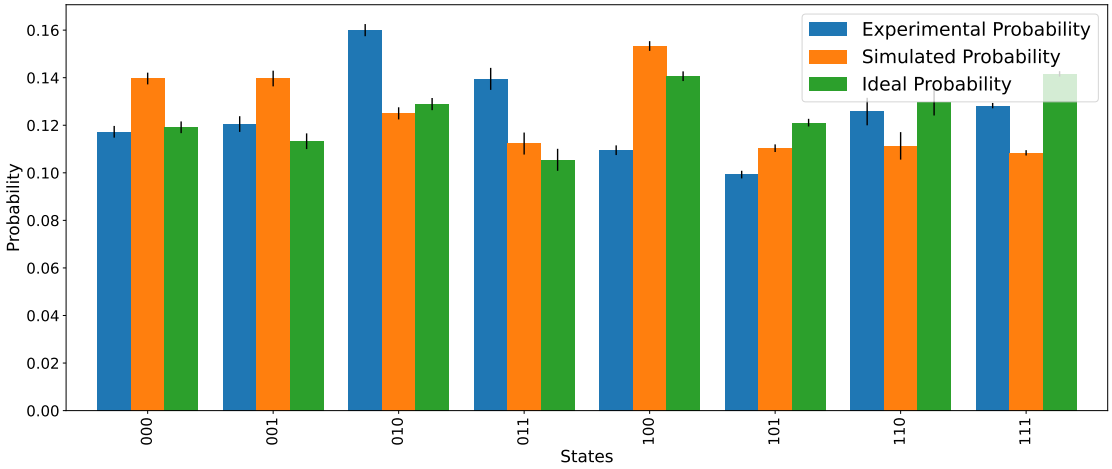

Figure 70: Hamiltonian circuit on Quito backend